Available online at www.sciencedirect.com

ScienceDirect

Geochimica et Cosmochimica Acta 292 (2021) 188–202

Geochimica et Cosmochimica Acta

www.elsevier.com/locate/gca

Carbon isotope evidence for the substrates and mechanisms of prebiotic synthesis in the early solar system

L. Chimiak [a,*], J.E. Elsila [b], B. Dallas [a], J.P. Dworkin [b], J.C. Aponte [b,c], A.L. Sessions [a], J.M. Eiler [a]

[a] Division of Geological and Planetary Sciences, California Institute of Technology, Pasadena, CA 91125, USA
[b] Solar System Exploration Division, Code 691, NASA Goddard Space Flight Center, Greenbelt, MD 20771, USA
[c] Department of Chemistry, Catholic University of America, Washington, D.C. 20064, USA

Received 27 April 2020; accepted in revised form 21 September 2020; Available online 29 September 2020

Abstract

Meteorites contain prebiotic, bio-relevant organic compounds including amino acids. Their syntheses could result from diverse sources and mechanisms and provide a window on the conditions and materials present in the early solar system. Here we constrain alanine's synthetic history in the Murchison meteorite using site-specific $^{13}C/^{12}C$ measurements, reported relative to the VPDB standard. The $\delta^{13}C_{VPDB}$ values of $-29 \pm 10‰$, $142 \pm 20‰$, and $-36 \pm 20‰$ for the carboxyl, amine-bound, and methyl carbons, respectively, are consistent with Strecker synthesis of interstellar-medium-derived aldehydes, ammonia, and low-$\delta^{13}C$ nebular or interstellar-medium-derived CN. We report experimentally measured isotope effects associated with Strecker synthesis, and use them to constrain the $\delta^{13}C$ values of the alanine precursors, which we then use to construct a model that predicts the molecular-average $\delta^{13}C$ values of 19 other organic compounds of prebiotic significance found in Murchison if they were made by our proposed synthetic network. Most of these predictions agree with previous measurements, suggesting that interstellar-medium-derived aldehydes and nebular and/or pre-solar CN could have served as substrates for synthesis of a wide range of prebiotic compounds in the early solar system.

Keywords: Meteorite Chemistry; Origins of Life; Strecker Synthesis; Site-Specific Isotope Ratios

1. INTRODUCTION

Carbonaceous chondrite (CC) meteorites contain amino acids (Cronin and Moore, 1971; Engel et al., 1990; Glavin et al., 2018), the extraterrestrial origins of which are evinced by their chemical and isotopic properties. Known life predominantly synthesizes 20 amino acids that are mostly L enantiomers and ~2% lower in their $^{13}C/^{12}C$ ratios than the average terrestrial inorganic carbon. On the other hand, the CC meteorites contain over 90 amino acids that are nearly racemic mixtures of D and L enantiomers—likely unchanged since their arrival on Earth—and are generally ~1–3% higher in their $^{13}C/^{12}C$ ratios than the average terrestrial inorganic carbon (Martins and Sephton, 2009; Burton et al., 2012; Elsila et al., 2016; Glavin et al., 2018).

Proposed mechanisms of meteoritic amino acid synthesis include *(i)* ion/radical-molecule reactions in the interstellar medium (ISM) (*e.g.*, with the irradiation of methanol ices (Bernstein et al., 2002)), *(ii)* Fischer-Tropsch type (FTT) synthesis in the protosolar nebula (Botta and Bada, 2002), and/or *(iii)* aqueous chemistry (*e.g.*, Strecker synthesis or reductive amination) of ISM-derived precursor molecules that were accreted in ices by the meteorite parent bodies and reacted during aqueous

* Corresponding author.
E-mail address: lchimiak@caltech.edu (L. Chimiak).

https://doi.org/10.1016/j.gca.2020.09.026
0016-7037/

alteration (Kerridge, 1999; Pizzarello et al., 2006; Glavin et al., 2018). The molecular-average $\delta^{13}C$ values[1] of individual α-amino acids from the Murchison CM2 CC decrease systematically with increasing carbon number (Pizzarello et al., 1991; Sephton, 2002; Elsila et al., 2012; Glavin et al., 2018), suggesting that they might have been assembled from smaller precursors with each newly added carbon atom being lower in ^{13}C than its source due to kinetic isotope effects (KIEs) (Yuen et al., 1984; Engel et al., 1990; Sephton, 2002). Alternatively, these trends could reflect the dilution of a high-$\delta^{13}C$ carbon atom inherited from ISM-derived CO by carbon from other, lower $\delta^{13}C$ precursors (Elsila et al., 2012). However, in the full set of prior $\delta^{13}C$ measurements of Murchison α-amino acids, $\delta^{13}C$ variations for individual amino acids compared between studies span a range equal to the extent of the proposed correlation between carbon number and $\delta^{13}C$ and so calls these explanations into question.

These and other hypotheses regarding the origins of meteoritic amino acids can be tested through observations of their site-specific carbon isotope distributions (*i.e.*, the $\delta^{13}C$ values of individual carbon positions in each molecule). Here we present site-specific $\delta^{13}C$ measurements of the three carbon sites in alanine extracted from a sample of Murchison and measured using novel techniques conducted with an Orbitrap mass spectrometer.

2. METHODS AND MATERIALS

2.1. Materials

2.1.1. Meteorite

We analyzed two samples of Murchison meteorite, a Methods Development sample (analyzed winter and spring 2018) and an Analytical sample (analyzed summer 2018). The Methods Development sample was a 5 g piece of Murchison from the Field Museum of Natural History via Clifford N. Matthews's research group that was known to be contaminated; although this contamination means that analytical results are of limited value, it provided a natural sample on which we could assess our novel analytical procedures. The Analytical sample was a 2.6 g sample from a different piece of Murchison and the same source; the sample has been described in Friedrich et al. (2018).

The D/L ratio of alanine from the methods development sample is 0.4, which is far from a pure racemic mixture's value of 1 or past measurements and therefore suggests a high proportion of terrestrial contamination. The D/L ratio of alanine from the analytical sample is 0.85, which agrees with past measurements of Murchison alanine (Cronin et al., 1995). The overall amino acid content of the Analytical sample is also similar to those measured previously in Murchison (Cronin and Moore, 1971; Martins and Sephton, 2009; Friedrich et al., 2018), which combined with the D/L ratios of amino acids in this sample suggest minimal terrestrial contamination.

2.1.2. Derivatization Materials

Alanine standards used in this study were Alfa Aesar L-alanine (99% Purity) and one sample of alanine synthesized by Strecker synthesis (Purity confirmed by NMR, Fig. S1) (hereafter, 'Strecker standard'). In methods development, we also used alanine purchased from VWR (Purity > 99%, Lot # 2795C477) as a standard. The Alfa Aesar standard was synthesized via microbial aspartate fermentation. The VWR alanine standard, which has similar site-specific $\delta^{13}C$ values, was synthesized by fermentation by Pseudomonas. Origins of the aspartate precursor are unknown, but Hoffman and Rasmussen (Hoffman and Rasmussen, 2019), who studied supplier-bought alanine samples, demonstrate that in two different samples $\delta^{13}C$ of all sites are within 10‰ of each other. Calibration of standards is described in Appendix A. Ultrapure water was obtained from a MilliPore ultrahigh-purity water (18.2 MΩ cm; hereafter 'water') system at Caltech. In addition to the standards listed above, alanines with 99% ^{13}C label at C-1, C-2, or C-3 were purchased from Sigma Aldrich (C-1: Lot # EB2220V, C-2: Lot # SZ0643V, C-3: Lot # EB2211V).

Reagents used in derivatization reactions and cleaning at Caltech included: anhydrous methanol (MeOH; >99.8% purity, Macron Fine Chemicals, Batch# 0000042997), n-hexane (>98.5% purity, Millipore Sigma, HPLC grade, multiple lots), acetyl chloride (AcCl; >99% purity, Sigma Aldrich, Lot# BCBT8141), trifluoroacetic anhydride (TFAA; >99% purity, Sigma Aldrich, Lot# SHBJ0051), and dichloromethane (DCM, Sigma Aldrich, HPLC Plus, >99.9% purity). All derivatizing reagents were tested for amino acid contamination prior to use on samples (See Appendix B section for more details).

Prior to derivatization, glassware was cleaned with ultrapure water and combusted twice at 450 °C. The second combustion occurred the night before use and with no other glassware present. GC vial PTFE caps were new and handled with forceps that were pre-cleaned with methanol. Any cap whose interior was touched with forceps was discarded. Fumehoods and tubing for nitrogen gas were cleaned prior to derivatization. BioPur pipette tips were used on pipettes to prevent contamination. Chemical lab syringes (Hamilton, 250 μL) were cleaned with methanol prior to and after derivatization reactions, and instrument inlet syringes (Hamilton, 10 μL) were cleaned with 30 μL hexane and 30 μL DCM between and before all analyses.

2.2. Methods

2.2.1. Amino acid extraction

Amino acids were extracted from meteorite samples at NASA Goddard Space Flight Center (GSFC) following the protocol from (Elsila et al., 2012). Briefly, each sample was ground to a homogenized powder and sealed in a glass ampoule with 1 mL ultrahigh purity water (Millipore Integral 10 UV, 18.2 MΩ cm, <3 ppb total organic carbon) for

[1] $\delta^{13}C$ quantifies the ratio of $^{13}C/^{12}C$ relative to a standard, Vienna Pee Dee Belemnite (VPDB). Mathematically, $\delta^{13}C_{VPDB} = \frac{13_C/12_{C_{sa}}}{13_C/12_{C_{st}}} - 1$ where *sa* denotes the sample and *st* the VPDB standard, which has a ^{13}R value of 0.01118 (Brand et al., 2010). $\delta^{13}C$ is conventionally reported in parts per thousand (‰), *i.e.*, $\delta^{13}C = \left[\frac{(C_{13}/C_{12})_{sa}}{(C_{13}/C_{12})_{st}} - 1\right] \times 1000$

24 hours at 100 °C. The water extract was separated, dried under vacuum, and hydrolyzed in 6 N HCl vapor (Sigma Aldrich, double distilled) for 3 hours at 150 °C. This hydrolyzed extract was then desalted on a cation-exchange resin column (AG50W-X8, 100–200 mesh, hydrogen form, Bio-Rad), with the amino acids recovered by elution with 2 M NH_4OH (prepared from ultrahigh purity water and NH_3 (g) *in vacuo*); this eluent was split into two fractions and dried under N_2. The Methods Development sample was processed in this way in November 2017 and the analytical sample in May of 2018.

Upon arrival at Caltech, extracts were triple bagged, boxed, and stored in a freezer. One extract from the Methods Development sample was derivatized and analyzed in December 2017; the other was derivatized and analyzed in March 2018. A portion of each derivatized extract from the Methods Development sample was sent back to GSFC along with derivatized standards for secondary analysis. The extract from the Analytical sample was split between GSFC (85%) and Caltech (15%). Analyses were made on the analytical sample in June 2018 at GSFC and between June to July 2018 at Caltech.

2.2.2. Derivatization

A flow chart for handling of samples and blanks are depicted in Fig. S2. First, 1.0 mL of water:MeOH (3:1) was added to the centrifuge vials containing meteorite extract that had been shipped from GSFC. Vials with the Methods Development samples were capped, placed in a beaker of water, and sonicated for five minutes. The analytical sample extract sat in the water-methanol mixture for 20 minutes but was not sonicated. Samples were then uncapped and transferred into 2 mL GC vials ('sample vials') via combusted glass pipettes. All original shipped extract vials were rinsed twice more with the 3:1 water-methanol mixture without sonication. The rinse liquid was again transferred into the sample vials via glass pipette. Between the second and third rinse and following the third rinse, GC samples vials were dried under slow N_2 flow.

Standards and Murchison extract samples were then derivatized as N-trifluouroacetyl-O-methyl esters. Samples were brought up in 100 μL of anhydrous MeOH and placed in an ice bath. Using a clean syringe, 25 μL of AcCl was added dropwise to the sample, which was swirled between drops to limit localized boiling (the reaction with AcCl is strongly exothermic). Forceps were used to lift vials and swirl them in order to minimize potential contamination. Samples were capped and heated to 70 °C in a heating block for 1 hour. Samples were then cooled and dried under N_2. To avoid cross-contamination, all samples, blanks, and standards were dried separately. Next, 120 μL hexane and 60 μL TFAA were added and vials were capped and heated to 60 °C in a heating block for 30 minutes. Samples were evaporated under N_2 until 50 μL remained. We ended evaporation while ~100uL of solvent still remained to avoid evaporation of the amino acid derivatives. Following this, 500 μL hexane was added for the methods-development samples and 200 μL hexane was added for the analytical sample. In initial experiments on Alfa Aesar, VWR, and Strecker alanine derivatives, evaporation was carried out until only derivative remained, as determined by gravimetry. Isotopic analysis of these samples indicated that no site-specific carbon isotope effects occurred during evaporation (within measurement errors).

A split of the analytical sample extract and Caltech alanine standards were also derivatized as N-trifluoroacetate-O-isopropyl esters at GSFC following protocols from (Elsila et al., 2012) at GSFC. The methods are similar to those listed above but use isopropanol instead of methanol.

2.2.3. Amino acid characterization

Amino acid abundance and enantiomeric composition (*e.g.*, abundances of D- and L-alanine) of both the method development and analytical samples were measured at GSFC via liquid chromatography with fluorescence detection and time-of-flight mass spectrometry (LC-FD/ToF-MS) using methods described in (Glavin et al., 2010). For the methods development samples, 1% of the sample was used for amino acid characterization, while for the analytical sample, 0.4% of the initial 2.6 g sample was used for characterization (details in (Friedrich et al., 2018)).

2.2.4. Isotope ratio measurements

2.2.4.1. Molecule-average isotope analysis of Murchison samples. Approximately 99% of the methods development sample was sent as two splits to Caltech where it was derivatized as N-trifluoroacetate-O-methyl ester (See *2.2.2:* Derivatization for further details) on the two analysis dates (winter and spring 2018). One aliquot of each derivatized sample in addition to two derivatized standards (Strecker and Alfa Aesar) were sent back to GSFC where they were analyzed for molecular-average (combining both chiral forms) $\delta^{13}C$ via Gas Chromatography-Combustion-IRMS (GC-C-IRMS) with a TC-5LIMS 30 m column. For the analytical sample, the 85% that remained at GSFC was derivatized as N-trifluoroacetate-O-isopropyl ester and injected into a GC–MS with four 25 m Chirasil-L-Val columns (Agilent, CP7495) connected in series. This long chiral column allowed us to separate and measure the $\delta^{13}C$ values of D- and L-alanine.

2.2.4.2. Site-specific isotope analysis. Site-specific carbon isotope ratios of derivatized alanine samples and standards were measured at Caltech The constraints presented in this paper are based on measurements of the bulk carbon isotope ratio of the full molecule by GC-combustion IRMS (yielding the average $\delta^{13}C$ of C-1, C-2, and C-3), along with direct mass spectrometric measurements of $^{13}C/^{12}C$ ('^{13}R') of two fragment ions of the alanine derivative, one of which constrains the average ratio for C-1 and C-2 and the other of which constrains the average ratio for C-2 and C-3. For carbon number identities, see Fig. 1. These three independent constraints permit us to calculate the $\delta^{13}C$ of each of C-1, C-2 and C-3 (see *2.3*: Data Processing).

The fragment ion measurements were made using the Q-Exactive GC Orbitrap mass spectrometer (hereafter 'Orbitrap'), using techniques described in (Eiler et al., 2017). The Orbitrap can mass resolve a ^{13}C substitution from D, ^{15}N, or ^{17}O substitutions allowing a user to measure the ^{13}R of a fragment directly (*e.g.* without combusting a fragment and then converting carbon into CO_2) (Fig. 1c and d

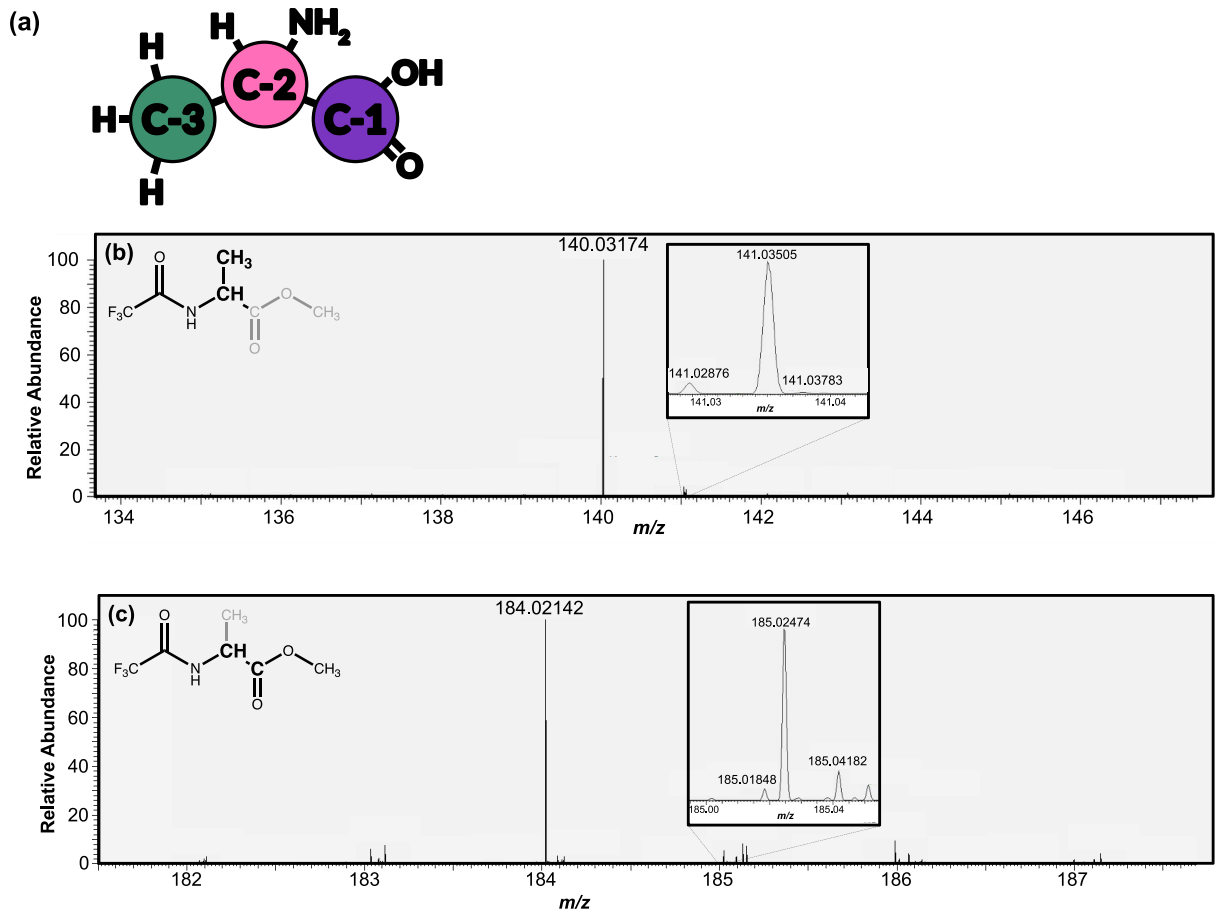

Fig. 1. Mass spectra and fragment images for alanine from Murchison meteorite sample measured in this study. (a) Alanine with carbon sites are labelled. Mass spectra and labelled fragment images are presented for (b) *m/z* 140 and (c) *m/z* 184. In panels (b) and (c), fragments are in black with the rest of the derivative in gray, and carbon sites from alanine being measured are bolded. Insets for each mass spectra displays ^{13}C-substituted peak to demonstrate resolution from potential isobars.

insets). The measured fragment ions have monoisotopic peaks (*i.e.*, the isotopologue containing only the most abundant isotope of each element, also known as the 'unsubstituted' isotopologue) of mass/charge (*m/z*) 140.0317 ($C_4H_5ONF_3$) and 184.0214 ($C_5H_5O_3NF_3$) Da (Fig. 1). Measurements of their isotope ratios will be referred to by their monoisotopic mass (*i.e.*, 140.032 for the $^{13}C/^{12}C$ ratios derived from ions with masses 141.0350 and 140.0317 Da). The relative contributions of the carbon sites from the parent molecule to each fragment ion were determined by analyzing three mixtures, each with a 10% ^{13}C enrichment at one carbon site (produced by mixing an appropriate site-specific, 99% labeled alanine with the unlabeled standard). The $m/z = 140.032$ fragment contains both C-2 and C-3 from the parent alanine along with two carbons from the TFAA reagent (Fig. 1c). The $m/z = 184.021$ fragment contains C-1 and C-2 from parent alanine along with all three carbons from the derivatizing reagents (Fig. 1d). From labelling studies, both appear to be direct fragmentation products with no obvious evidence for recombination reactions that may add carbon atoms from one sample site into a different molecular ion.

The methods of high-precision isotope ratio analysis by Orbitrap-based mass spectrometry are described in Eiler et al. (2017). For the measurements presented in this paper, two configurations were used: direct analysis of analyte peaks eluting from a GC column ('Direct Elution') and analyte capturing from the GC effluent into a reservoir followed by isotopic analysis as it drained from that reservoir ('Reservoir Elution') (Fig. 2). The Direct Elution mode was used to characterize the fragmentation pattern and retention time of derivatized alanine (Fig. 2c). For this study, analyte eluting from the GC column was admitted to the ion source continuously following a 5.5-minute delay to avoid the solvent peak. Pre-mass selection using the AQS (quadrupole) system was set to permit all ions between *m/z* 50 and 300 Da to enter the Orbitrap mass analyzer. Reservoir Elution mode was used to measure ion-abundance ratios at a useful precision for study of natural stable isotope variations. Here Reservoir Elution mode measurements were conducted with an initial 5.5-minute solvent delay followed peak monitoring in Direct Elution mode until 30 seconds prior to the elution of derivatized alanine, which could be timed relative to the retention times of

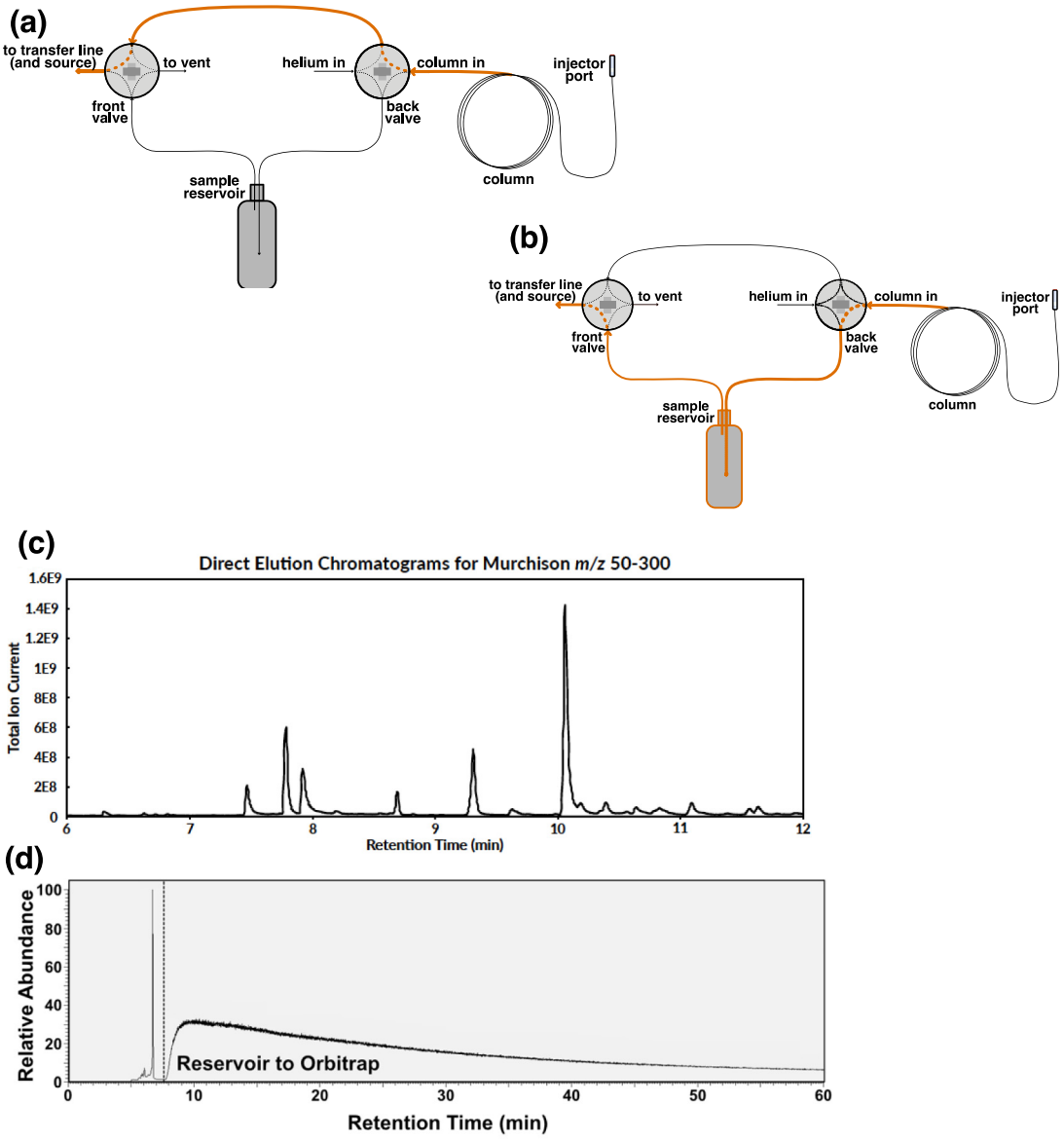

Fig. 2. Schematic of custom inlet system for Orbitrap for (a) direct injection and (b) reservoir elution. (c) Chromatogram of 50–300 Da for direct injection that was used to find elution of alanine in Murchison sample. (d) Chromatogram of the 140.032 Da peak for reservoir elution during a typical measurement for Murchison sample.

earlier-eluting compounds (Fig. 2d). At this point, the effluent from the GC column was rerouted into either a 5 or 20 cm^3 glass reservoir, the contents of which were flushed with He into the ion source. The 20 cm^3 reservoir was used for measurements of the relatively high intensity 140.032 fragment and the 5 cm^3 reservoir was used for the weaker intensity 184.021 and 113.021 fragments, in order to increase signal-to-noise ratios (For more information on the 113.021 fragment, see Appendix C). Following the total collection of the derivatized alanine peak, GC column effluent was vented and clean helium was directed into the reservoir to continue purging analyte into to the ion source for the remainder of the measurement. In this fashion the glass reservoir serves as an exponential-dilution flask (Merritt and Hayes, 1994) that broadens the analyte peak from a few seconds to tens of minutes and thereby facilitates the accumulation of more ion counts – and thus greater precision for isotope ratios – by the Orbitrap. Alanine measurements were accumulated for 10- to 60-minutes depending on the reservoir size and the abundance of the fragments of interest (Fig. 2d).

For detailed information on blanks and background analysis see Appendix B. In short, background scans were taken prior to each set of Murchison injections to ensure that no background alanine was present at intensities that could significantly impact the measured isotope ratios of the sample. In cases in which alanine or other contaminants were present in the reservoir or column, solvent blanks were

run with only helium entering the reservoir until backgrounds subsided. Measurements of $^{13}C/^{12}C$ displayed no evidence of drift over the period of days during which the data was acquired (Electronic Annex 1) and measurements of the Strecker standard's $\delta^{13}C$ of the C-2 + C-3 sites directly following those of the Alfa Aesar standard were within 2 standard errors of independently known values (Appendix A). These factors suggest an absence of memory effects in the instrument.

Orbitrap measurements produce a series of 'scans', each of which reports the apparent ^{13}R of a selected fragment (*i.e.*, for the $m/z = 140.032$ or 184.021 fragments; see values in Electronic Annex 1). Measurements begin when the alanine peak elutes (*i.e.*, when the NL of the monoisotopic peak is at its minimum immediately prior to alanine's elution). To minimize mass spectrometric artifacts (Eiler et al., 2017), we accept only those analyses in which both the monoisotopic and singly ^{13}C-subsituted fragments are present, in which the monoisotopic ion makes up at least 30% of the total ion current (TIC) in the observed mass window (Electronic Annex 1), and in which the product of the TIC and injection time (IT) varies over a narrow range (~10′s of %, relative) between scans. In some cases, the trace of ion intensities provides evidence that we failed to capture all of the alanine peak in the reservoir and/or a nearly co-eluting peak has been captured with it (*e.g.*, in the case of the 113.021 peak of the Murchison sample discussed in Appendix C); these measurements are also discarded as procedural failures. Standard errors were calculated as the standard deviation of all accepted scans ^{13}R values for a fragment divided by the square root of the number of scans for that fragment.

The accuracy and precision of site-specific measurements was verified via a comparison of differences in $\delta^{13}C$ of C-1 measured by the Orbitrap with that measured by ninhydrin decarboxylation for the three standards (See Appendix A for a detailed discussion). The average $\delta^{13}C$ values for C-2 and C-3 of Strecker alanine relative to the Alfa Aesar alanine standard measured by the 140.032 Da fragment on the Orbitrap during our experiments was $-17.4 \pm 1.6‰$ (See Appendix D for Error Analysis). This value is just beyond 2 standard errors from the value found from subtraction of $\delta^{13}C$ C-1 from the molecular-average $\delta^{13}C$ measured by ninhydrin decarboxylation and molecular-average EA-IRMS measurements for Strecker alanine relative to the Alfa Aesar alanine standard ($-13.4 \pm 0.6‰$).

Differences in the isotopic composition between the Alfa Aesar and Strecker standards' fragments were constant within the nominal external errors of each measurement over the course of our analysis (Electronic Annex 1) and between analysis sets (Table 1). Each standard had stable measurements of each fragment's ratios of the ^{13}R over the course of our measurements: when source backgrounds are low, the standard deviation for Alfa Aesar's ^{13}R between different injections normalized to the measurements' averages are 4.6‰ and 14.0‰ for the m/z 140.032 and 184.021 fragments, respectively, for quantities of analyte similar to those of Murchison extracts. Furthermore, the variation decreases with increasing quantity of analyte (*i.e.*, the samples that most vary from the mean tend to be of lower intensity fragments and/or measurements) because ^{13}C counts increase with analyte quantity, and the instrument's shot noise limit is inversely proportional to the square root of the number of ^{13}C counts.

We tested our ability to trap and analyze derivatized alanine in amino acid mixtures by measuring alanine in a standard mixture comprising the 20 most abundant amino acids in Murchison in relative abundances that match those in Martins and Sephton (Martins and Sephton, 2009), as well by measuring alanine in the methods development sample in two analytical periods. We used the Alfa Aesar alanine standard in the standard mixture and compared it to measurements of pure Alfa Aesar alanine (*i.e.* not in a mixture) to ensure that the methodology used to measure mixtures would not fractionate alanine. The standard mixture was handled in a manner similar to that of the meteorite samples including being transferred in a water methanol mixture and dried down prior to derivatization. Relative to the Alfa Aesar standard, the standard mixture had a $\delta^{13}C$ of 2‰, which was within error of its measurement. Furthermore, excepting one methods development sample that was contaminated during derivatization (November 2017), the averaged C-2 + C-3 $\delta^{13}C$ (*i.e.*, that of the 140.032 Da fragment) and the averaged C-1 + C-2 $\delta^{13}C$ (184.021 Da fragment) values for two aliquots of methods development measured via GC-C-IRMS at GSFC and on the Orbitrap at Caltech in January and March of 2019 were within error of one another (Table 1, Appendix A). The summer 2018 analysis of the Strecker alanine is also within one standard error of the spring and winter 2018 C-2 + C-3 averaged $\delta^{13}C$ value and C-1 + C-2 averaged $\delta^{13}C$ value.

2.3. Data processing

2.3.1. Calculations of site-specific isotope ratios

Several arithmetic operations were required to calculate the site-specific $\delta^{13}C$ values for C-1, C-2, and C-3 in alanine. First, all accepted analyses for each fragment were combined (see Section 2.2.4.1 for criteria of accepted scans and Table S3 for analyses used) and the ^{13}R of each fragment was calculated as a weighted average of all counts (monoisotopic and singly ^{13}C-substituted) for the fragment (Eqn. (1))

$$^{13}R_{frag} = \sum_{i=1}^{n} \left[{}^{13}R_{scan} \times \frac{{}^{12}C_{cts,scan} + {}^{13}C_{cts,scan}}{\Sigma^{12}C_{cts,scan} + \Sigma^{13}C_{cts,scan}} \right]_i \quad (1)$$

where $^{13}R_{frag}$ is the ^{13}R value used for a fragment measurement, $^{13}R_{scan}$ is the ^{13}C counts/^{12}C counts for a single scan as defined in Eiler et al (2017) with a C_N (the charge conversion constant) of 3.6, $^{x}C_{cts,scan}$ is the and number of counts of isotope, *x,* for a single scan. The measurement is summed over all included scans.

This $^{13}R_{frag}$ value was then converted into $\delta^{13}C_{VPDB}$. To this end, the measured $^{13}R_{frag}$ of each fragment was standardized to Alfa Aesar by dividing the sample's $^{13}R_{frag}$ by that of Alfa Aesar alanine for the same fragment ion measured under the same analytical conditions (*i.e.*, same elution times into reservoir, same AGC conditions, similar TICxIT ranges) and temporally close (*i.e.*, same

Table 1
Fragment ^{13}R values and $\delta^{13}C$ values (AA and VPDB scales) for samples, standards, blanks. All delta values are dilution corrected. Standard error values are listed in parentheses. The first two columns of data (Molecular-average $\delta^{13}C$ and Fragment ^{13}R) were directly measured while Fragment $\delta^{13}C$ values relative to Alfa Aesar and VPDB were calculate using equation S1. The $\delta^{13}C$ values used in the Monte Carlo simulation are in the last columns (Fragment $\delta^{13}C_{VPDB}$).

Analysis set	Sample	Molecular average $\delta^{13}C_{VPDB}$ (‰)	Fragment ^{13}R (‰)		Fragment $\delta^{13}C_{AlfaAesar}$ (‰)		Fragment $\delta^{13}C_{VPDB}$ (‰)	
			140	184	140	184	140	184
Winter 2018	Alfa Aesar	−19.4 (0.2)	0.04313 *(0.00004)*	0.05392 *(0.00018)*	x	x	x	x
	Strecker	−32.9 (0.1)	0.04297 *(0.00004)*	0.05381 *(0.00012)*	−7.4 *(2.8)*	−5.5 *(9.9)*	**−22.1** *(2.8)*	**−27.0** *(9.9)*
	Methods Development Murchison	17 (4)	0.04379 *(0.00004)*	0.05458 *(0.00020)*	30.5 *(2.8)*	30.3 *(12.2)*	**15.3** *(2.8)*	**8.0** *(12.2)*
Spring 2018	Alfa Aesar	−19.4 (0.2)	0.04323 *(0.00003)*	0.05389 *(0.00028)*	x	x	x	x
	Strecker	−32.9 (0.1)	0.04289 *(0.00002)*	x	−15.5 *(2.0)*	x	**−30.1** *(2.0)*	x
	Methods Development Murchison	17 (4)	0.04381 *(0.00003)*	0.05503 *(0.00024)*	27.3 *(2.1)*	53.0 *(18.9)*	**12.1** *(2.1)*	**30.3** *(18.9)*
Summer 2018	Alfa Aesar	−19.4 (0.2)	0.04237 *(0.00002)*	0.05538 *(0.00010)*	x	x	x	x
	Strecker	−32.9 (0.1)	0.04203 *(0.00003)*	0.05493 *(0.00018)*	−16.0 *(1.8)*	−20.2 *(9.3)*	**−30.5** *(1.8)*	**−41.4** *(9.2)*
	Analytical Murchison	25.5 (3)	0.04382 *(0.00003)*	0.05714 *(0.00017)*	68.4 *(1.5)*	79.8 *(8.9)*	**52.6** *(1.5)*	**56.4** *(8.9)*

measurement period). The standardized $^{13}R_{frag}$ for the alanine carbon site(s) in a fragment were then corrected for the dilution by carbon(s) from derivatizing reagents present in the fragment of interest (as these carbons have the same source in the sample and standard; see Table 1). This correction is found in equation (2):

$$^{13}R_{corr} = \left(\left(\left(\,^{13}R_{sa,meas}/\,^{13}R_{AA,meas} - 1\right) \times nC_{frag}/nC_{ala}\right) + 1\right) \times \,^{13}R_{AA,fVPDB} \quad (2)$$

where $^{13}R_{corr}$ is the standardized ^{13}R value for a given fragment, $^{13}R_{sa,meas}$ is the $^{13}R_{frag}$ value for a sample directly measured for a fragment on the Orbitrap, $^{13}R_{AA,meas}$ is the $^{13}R_{frag}$ value for the Alfa Aesar standard directly measured for the same fragment on the Orbitrap, nC_{frag} is the total numbers of carbons in a fragment (*e.g.* 4 carbons for the 140.035 fragment), nC_{ala} is the numbers of carbons from alanine in that fragment (*e.g.* 2 carbon for the 140.035 fragment), and $^{13}R_{AA,fVPDB}$ Alfa Aesar's ^{13}R value for the alanine carbons in the fragment on the VPDB scale (for more information on these values see Eiler et al. (2017). Finally, the standardized and corrected ^{13}R values were transcribed into $\delta^{13}C_{VPDB}$ values (Table 1). The corrected values assume that the derivative carbons between samples and standards have the identical ^{13}R values at each site between sample and standard (*i.e.*, such that ratios may be treated as conservatively mixed properties) and that they have the same $\delta^{13}C$ values as the Alfa Aesar standards. We examined this assumption and found that variations less than ~50‰ would result in errors below the analytical uncertainty. Using corrected ^{13}R values for each fragment ion, we found the $\delta^{13}C_{VPDB}$ value (See Footnote 1 for formula and description).

Once each fragment was assigned a $\delta^{13}C_{VPDB}$ value, we calculated the site-specific $\delta^{13}C_{VPDB}$ of each of the three alanine sites. Our measurements of the analytical sample extracts provided three independent constraints on the site-specific $\delta^{13}C$ values of alanine: the molecule-average isotope ratio measured by compound-specific GC-C-IRMS and the two ratios measured by the Orbitrap (for the 140.032 and 184.032 Da fragment ions). The assumption that derivative carbons are the same in the sample as the alanine standard provided a fourth constraint. Each constraint is associated with its own uncertainty and weighted effect on the $\delta^{13}C$ of each alanine carbon site.

For the site-specific isotope calculation, the GC-C-MS measurement of molecular-average $\delta^{13}C$, and the Orbitrap measurements of the averaged C-1 + C-2 and the averaged C-2 + C-3 $\delta^{13}C$ were converted to fractional abundances ($^{13}F_{avg}$, $^{13}F_{C1+C2}$, $^{13}F_{C2+C3}$ respectively) using the relation $^{13}F = {}^{13}R/(1 + {}^{13}R)$. The ^{13}F values were then used to solve the following set of mass balance expressions (Eqn. 3a-3c):

$$13_{F_{C-1}} = 3 \times 13_{F_{molecavg}} - 2 \times 13_{F_{C-2+c-3}} \quad (3a)$$

$$13_{F_{C-2}} = 2 \times 13_{F_{C-2+c-3}} 13_{F_{C-1}} \quad (3b)$$

$$13_{F_{C-3}} = 2 \times 13_{F_{C-2+c-3}} 13_{F_{C-2}} \quad (3c)$$

Once fractional abundances of ^{13}C in each site were calculated, they were converted $\delta^{13}C$ values. Error analysis is discussed in Appendix D.

3. RESULTS

The 267 ng sample of alanine recovered from an acid-hydrolyzed hot water extract of the Murchison sample studied here comprises 0.665 ppm by weight of the bulk meteorite, is a nearly racemic mixture of D and L enantiomers, and has molecular-average $\delta^{13}C_{VPDB}$ values of 25 ± 3‰ and 26 ± 3 ‰ for the D and L enantiomers, respectively, which is consistent with prior measurements of alanine from samples of Murchison (Engel et al., 1990; Martins and Sephton, 2009; Elsila et al., 2012). Acid hydrolysis increases yield in our samples from 2.37 ± 0.23 and 2.30 ± 0.16 nmol/g (water-extractable, or 'free' alanine) to 5.30 ± 0.88 and 5.98 ± 1.03 nmol/g (total alanine) for D- and L-alanine respectively (Friedrich et al., 2018). Past studies have demonstrated that 'free' and total alanine are indistinguishable in $\delta^{13}C$ ((Burton et al., 2013); similar results are found for other water-soluble organics as with (Aponte et al., 2014)). Procedural blanks typically yielded alanine abundances that were less than 1% of the recovered meteoritic material (see Appendix B, Fig. S3, and Tables S1 and S2). Although the enantiomeric proportions of amino acids cannot conclusively establish their biogenicity, the weight of the preceding observations lead us to conclude our sample contains no detectable terrestrial contamination and closely approaches the properties of indigenous alanine found in Murchison. The site-specific $\delta^{13}C$ values for alanine are -29 ± 10 ‰, 142 ± 20 ‰, and -36 ± 20 ‰ for the C-1, C-2, and C-3 sites, respectively (Table 2, see Fig. 1a for carbon site identities). Errors in each site-specific value are highly correlated due to the more precisely known molecular-average value (25.5 ± 3 ‰) and even more precisely known average of the C-2 and C-3 sites (52.6 ± 1.5 ‰); see the Appendix A for details. The carbon isotope structure we observe for Murchison alanine, particularly the marked ^{13}C enrichment of the C-2 site, provides new constraints on the mechanism, precursors, and setting of its synthesis.

4. DISCUSSION

4.1. Alanine formation mechanism

Isotopic measurements of compounds in the ISM, including the local ISM (*i.e.*, within 800 parsecs of the Sun (Lallement et al., 2018), which is at 7.94 ± 0.42 kiloparsecs from the galactic center (Eisenhauer et al., 2003)), exhibit large gradients in the $^{13}C/^{12}C$ of gas-phase carbon pools depending, in part, on their location in a molecular cloud. Furthermore, due to the high (hundreds of per mil) error associated with the measurements, the $^{13}C/^{12}C$ of most carbon pools (CO, CH_x, CN, CS) overlap. Consequently, for our analysis, we rely on the models of Charnley et al. (2004), which combine recent theories of ISM carbon chemistry and related isotope fractionations. Future measurements from higher precision instruments will allow for more refined isotopic models of ISM chemistry and thus will test our hypothesized reaction network and/or lead to refinements of our interpretation. Charnley et al.'s model and others predict CO will be highly ^{13}C enriched due to its high prevalence and the 35 K lower zero-point energy of ^{13}CO relative to ^{12}CO, as shown in equation (4).

$$^{12}CO + {}^{13}C^{+} \leftrightarrows {}^{13}CO + {}^{12}C^{+} + 35\ K \quad (4)$$

In the cold ISM, where temperatures are 10–40 K, this energetic difference drives ^{13}C into the CO pool and depletes the C^+ and CH_x pools in ^{13}C. One possible exception is CN, which has been modeled to have a $\delta^{13}C$ value that is either similar to the ^{13}C-enriched CO or to the ^{13}C-depleted C^+-derived pools of carbon-bearing molecules (Langer et al., 1984; Langer and Penzias, 1990; Milam et al., 2005). We note that, the only measurements of CN are: (1) KCN from the Murchison meteorite, which has a $\delta^{13}C$ value of 5 ± 3 ‰ (Pizzarello, 2014)—^{13}C-depleted relative to the CO-bearing molecule formaldehyde; and (2) cometary HCN that was measured to have a $H^{12}CN/H^{13}CN$ ratio of 88 ± 18 (*i.e.*, a $\delta^{13}C$ of $\sim 16^{+262}_{-172}$‰), which is within error of the solar system value of 89 (Cordiner et al., 2019). In both cases, the CN reservoir in the solar system does not bear enrichments predicted in Milam et al (2005), supporting the hypothesis that it is isotopically light — like the C^+ and CH_x pools. However, we note the possibility that the CN measured was not made in the ISM and that the error associated with the cometary HCN could place it in either the isotopically enriched or light pools.

When describing sources of precursor compounds in the ISM in our hypothesized reaction network, we consider two main pools: ^{13}C-enriched (CO and possibly CN) and ^{13}C-poor (CH_x and possibly CN). The first pool includes carbonyl carbons such as those in aldehydes and the second includes reduced carbon such as hydrocarbons and aliphatic carbon chains. Due to the cold temperatures leading to these isotopic fractionations between reservoirs, we would consider a ^{13}C value that is above 50‰—the predicted $\delta^{13}C$ reservoir for planets of 0‰ plus a potential 50‰ ^{13}C enrichment from isotope effects associated with synthesis (Lyons et al., 2018)—to likely include carbon derived from material that is either sourced from CO and/or CN in the ISM or in the outer solar system, which experiences similarly cold temperatures. Our finding of a $\delta^{13}C$ value that exceeds 100‰ at the C-2 site in alanine provides a strong indication that this site is derived from a precursor that was itself synthesized in the ISM from CO and its products and/or CN.

Our finding of a relatively low $\delta^{13}C$ value of the C-1 site, however, is inconsistent with current experimental constraints on amino acid synthesis via the irradiation of methanol ices and ammonia in the ISM. An experimental irradiation of isotopically labelled methanol ices at 40 K (Elsila et al., 2007) produced adequate amounts of serine for site-specific analyses and found that both the C-1 and C-2 sites are inherited from HCN, implying that this mechanism should not lead to marked differences between the carbon isotopic compositions of the C-1 and C-2 sites.

Table 2
Fragment and site-specific $\delta^{13}C_{VPDB}$ values for hydrolyzed alanine from a Murchison meteorite hot water extract and the Strecker standard. The full molecular-average direct measurement $\delta^{13}C$ value was measured via GC-C-IRMS, and the fragments' $\delta^{13}C$ values were measured on the Q-Exactive GC Orbitrap mass analyzer. The site-specific $\delta^{13}C$ values were calculated using the average of the D- and L-alanine molecular averages and the fragment $\delta^{13}C$ values (see Methods 2.3.1 for details on calculations).

	Carbon site(s)	$\delta^{13}C_{VPDB}$ (‰)	*st err (‰)*	$\delta^{13}C_{VPDB}$ (‰)	*st err (‰)*
Direct measurement	L-Alanine Molecular Avg.	26	*3*	*−32.1*	*0.1*
	D-Alanine Molecular Avg.	25	*3*		
	Average of C-1 and C-2	56.4	*8.9*	−30.5	*1.8*
	Average of C-2 and C-3	52.6	*1.5*	−41.4	*9.2*
Site specific calculations	C-1	−28.7	*9.5*	−37.7	*3.6*
	C-2	141.5	*20.1*	−45.1	*13.6*
	C-3	−36.3	*20.4*	−15.9	*13.9*

Assuming that alanine follows a similar formation pathway to serine, we conclude that alanine from Murchison inherited the C-2 carbon from a precursor that was itself formed from the CO, HCO^+, and/or CN pools in the ISM and that its ^{13}C depletion in the C-1 carbon was contributed from another, lower $\delta^{13}C$ precursor through reactions that likely occurred either in the early solar nebula or in Murchison's parent body. However, we note that further experiments should explore the potential to form alanine through alternate pathways in the ISM, such as by gas-phase reactions and gas-grain reactions, and that experiments should sample carbon sources in a manner that reflects the diversity found in in interstellar ices. Specifically, we note that ice-grain experiments presented in Elsila et al. (2007)) produced glycine that formed by multiple formation pathways, including a minor pathway in which C-1 was derived from HCN and C-2 from methanol — a pattern of transfer from substrate to amino acid sites that could be mistaken for the Strecker synthesis. Further experiments of this kind are required to determine the factors controlling the relative rates of the pathways of amino acid synthesis that can occur in ice grain chemistry, especially those that lead to synthesis of aliphatic α-H and α-CH_3 amino acids such as alanine or isovaline.

Our findings are also inconsistent with the hypothesis that this nebular or parent body chemistry followed a predominantly FTT mechanism. FTT-synthesized alanine inherits all its carbons from the source CO, with each added carbon being only subtly lower in $\delta^{13}C$ than the CO pool due to a KIE of approximately 0–10‰ (Mccollom and Seewald, 2006; Taran et al., 2007). Although this reaction mechanism is incapable of directly generating the ~170‰ contrast we observe between the $\delta^{13}C$ values of the C-2 site compared to the C-1 and C-3 sites, it is possible that alanine could form by an FTT-like process if the carbon in the C-2 site were derived from a secondary product of small molecules other than CO. In some conditions, FTT chemistry can create CO_2 and CH_4 that differ from one another by up to ~50‰ (Taran et al., 2007)— a contrast approaching that required by our data. In this case, alanine synthesis by FTT would require that the C-2 carbon is a secondary product of the ^{13}C-enriched CO_2 produced by FTT synthesis, whereas the C-3 and – most problematically – C-1 carbon are secondary products of low ^{13}C FTT-derived CH_4. We can think of no plausible chemical reaction sequences in which this would happen.

For these reasons, given the current understanding of isotope effects and mechanisms of interstellar and nebular chemistry, we conclude that alanine in Murchison likely formed via Strecker synthesis or reductive amination, that it was synthesized in the solar nebula, possibly in the meteorite's parent body, and that it had likely at least one reactant that itself was derived from CO or CN in the ISM or outer solar system. Drawing on past models and measurements, Elsila et al. (2012) and Aponte et al. (2017) argued that meteoritic alanine formed by Strecker synthesis from ISM-derived acetaldehyde with a ^{13}C-enriched carbonyl carbon inherited from CO and ^{13}C-depleted methyl carbon inherited from the CH_x pool, in addition to NH_3, and ^{13}C-depleted HCN such as that measured on Murchison. These reactants would lead to alanine with a high $\delta^{13}C$ value at the C-2 site and lower $\delta^{13}C$ at the C-1 and C-3 sites (Elsila et al., 2012) (Fig. 3). The results presented here are consistent with this argument. If instead alanine formed by reductive amination, one of its precursors would have been pyruvic acid. If the precursor were pyruvic acid formed solely by CO grain chemistry (Elsila et al., 2012), then all of its carbon sites and those on the subsequently produced alanine will be equally ^{13}C-enriched, in disagreement with our findings. If, however, pyruvic acid formed via a ketene or aldehyde reacting with HCN and water in the ISM (Cooper et al., 2011) or cyanohydrin in the parent body, it could result in a carbon isotope structure broadly resembling that produced by Strecker synthesis (See Appendix E). We consider these two mechanisms equally plausible based on the constraints of our alanine's C isotope structure. Non-α-amino acids (*e.g.*, β-, γ-) cannot be produced via the Strecker pathway and require other mechanisms of production.

4.2. Precursor reservoir values

To help us predict the isotopic contents and structures for the precursors to alanine in Murchison, we synthesized alanine via Strecker synthesis and measured its site-specific carbon isotope effects relative to the starting acetaldehyde and NaCN (see Table 3 and Appendix F). Experiments indicate that production of the α-aminopropanenitrile

intermediate has a $\delta^{13}C$ that is 10‰ below its acetaldehyde precursor at moderate (~60–70%) yields. Because the C-3 carbon does not gain or lose covalent bonds in the Strecker reaction, and thus will not experience large isotope effects from the synthesis, the 10‰ shift in the average C-2 and C-3 $\delta^{13}C$ value suggests a −20‰ isotope effect on the C-2 carbon (see Table 3, Fig. 3), which is consistent with the KIE on a carbonyl carbon from the addition of CN (Lynn and Yankwich, 1961). If we assume a large initial acetaldehyde reservoir such that its isotopic value is effectively constant during alanine production, and account for the reactant aldehyde's fractionation by adding 10‰ to the C-2 and C-3 site's average $\delta^{13}C$, we predict that the initial acetaldehyde reservoir parental to Murchison alanine had a molecular-average $\delta^{13}C$ of 62.6 ± 1.5‰. This value is within error of 64 ± 1‰, a molecular-average value for acetaldehyde recently measured in Murchison (Fig. 4, Electronic Annex 2, and (Aponte, Whitaker, et al., 2019)). This agreement is consistent with our suggestion that alanine had an acetaldehyde precursor and thus reinforces the possibility that alanine was synthesized by Strecker reaction rather than reductive amination; it also suggests that the initial aldehyde pool was not fractionated during the synthesis of alanine and was therefore either large in amount relative to the alanine produced or that aldehyde was continuously produced (*e.g.*, from the hydrolysis of other acetaldehyde-derived compounds) as it was consumed in alanine syntheses. We note that other measurements of the molecular-average $\delta^{13}C$ of acetaldehyde have found values of 25–27‰ (Simkus et al., 2019) possibly due to sample heterogeneity or fractionation of volatile molecules during laboratory extraction (Aponte, Whitaker, et al., 2019). Future site-specific isotope ratio studies of Strecker synthesis reactants (*e.g.*, aldehyde, CN) and products from the same sample could resolve the reason for this discrepancy and further test our hypothesis.

The Strecker experiments also indicate that the acid hydrolysis of α-aminonitrile to an amino acid has a KIE on the C-1 site of up to −50‰ for a 13% conversion of cyanide to alanine and a mean value of −22‰ for a 20–55% conversion of α-aminonitrile to alanine (Table 3, Fig. 4). Therefore, if alanine in Murchison formed by Strecker synthesis with moderate yield in its second step (20–50%), it should have inherited its C-1 carbon from reactant HCN that had $\delta^{13}C$ of −7 ± 10‰ (For error analysis, see Appendix D). This value is within error of the previously reported 5 ± 3‰ $\delta^{13}C$ of HCN in Murchison (Pizzarello, 2014). It is noteworthy that the HCN extracted from Murchison has a lower $\delta^{13}C$ than do formaldehyde and acetaldehyde from that sample: this difference is consistent with the idea that the HCN reservoir available on Murchison was ^{13}C-depleted relative to the reservoir that created the alpha site on α-amino acids. Other combinations of substrate $\delta^{13}C$ values and reaction yields are also possible, but the agreement of this scenario with independent constraints for acetaldehyde and HCN support its plausibility.

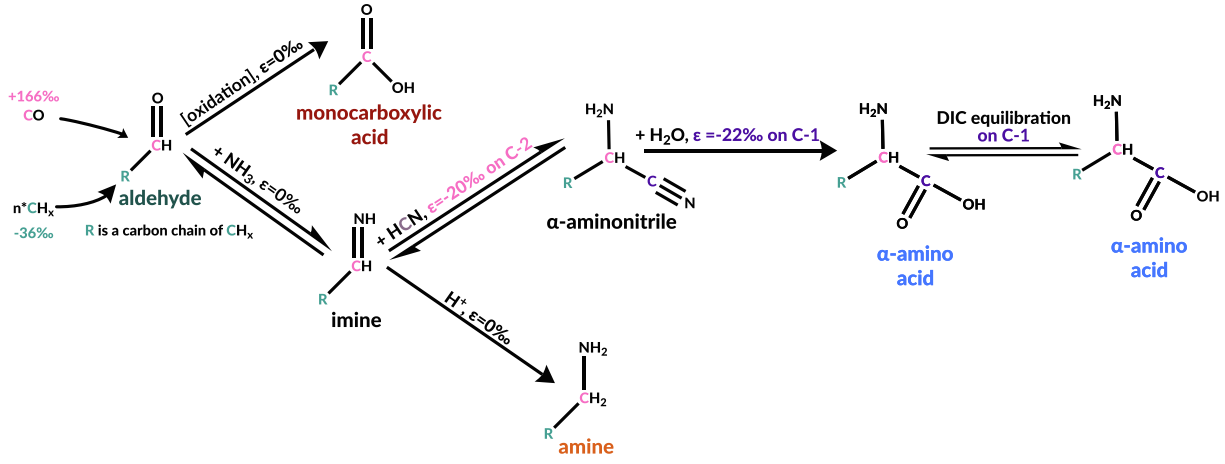

Fig. 3. Proposed mechanisms for syntheses of organic compounds related to alanine (with R of CH_3) on the Murchison parent body, with associated carbon isotope effects. In this scheme, CO and CH_x are derived from the ISM. Reaction steps between the aldehyde and imine and between the imine and aminonitrile are reversible (Van Trump, 1975). Isotopic values for the initial CO and $n$$CH_x$ are back-calculated using our measured alanine value and the isotopic effects shown.

Table 3
Site-specific isotope effects measured for the Strecker synthesis of alanine. The $\varepsilon_{C\text{-}1}$ likely has a non-zero value as exists for the equilibrium between CN and HCN, but in the experiments all CN was converted into 2-propionitrile so no isotope effect could be measured for the aminonitrile formation.

Mechanism step *(isotope effect type)*	$\varepsilon_{C\text{-}1}$ (‰)	$\varepsilon_{C\text{-}2\,+\,C\text{-}3}$ (‰)	$\varepsilon_{C\text{-}2}$ (‰)
Aminonitrile formation *(EIE)*	N/A	−10	−20
Aminonitrile hydrolysis to amide *(KIE)*	−8.5	0.7	1.4
Amide hydrolysis to amino acid *(KIE)*	−15	0	0

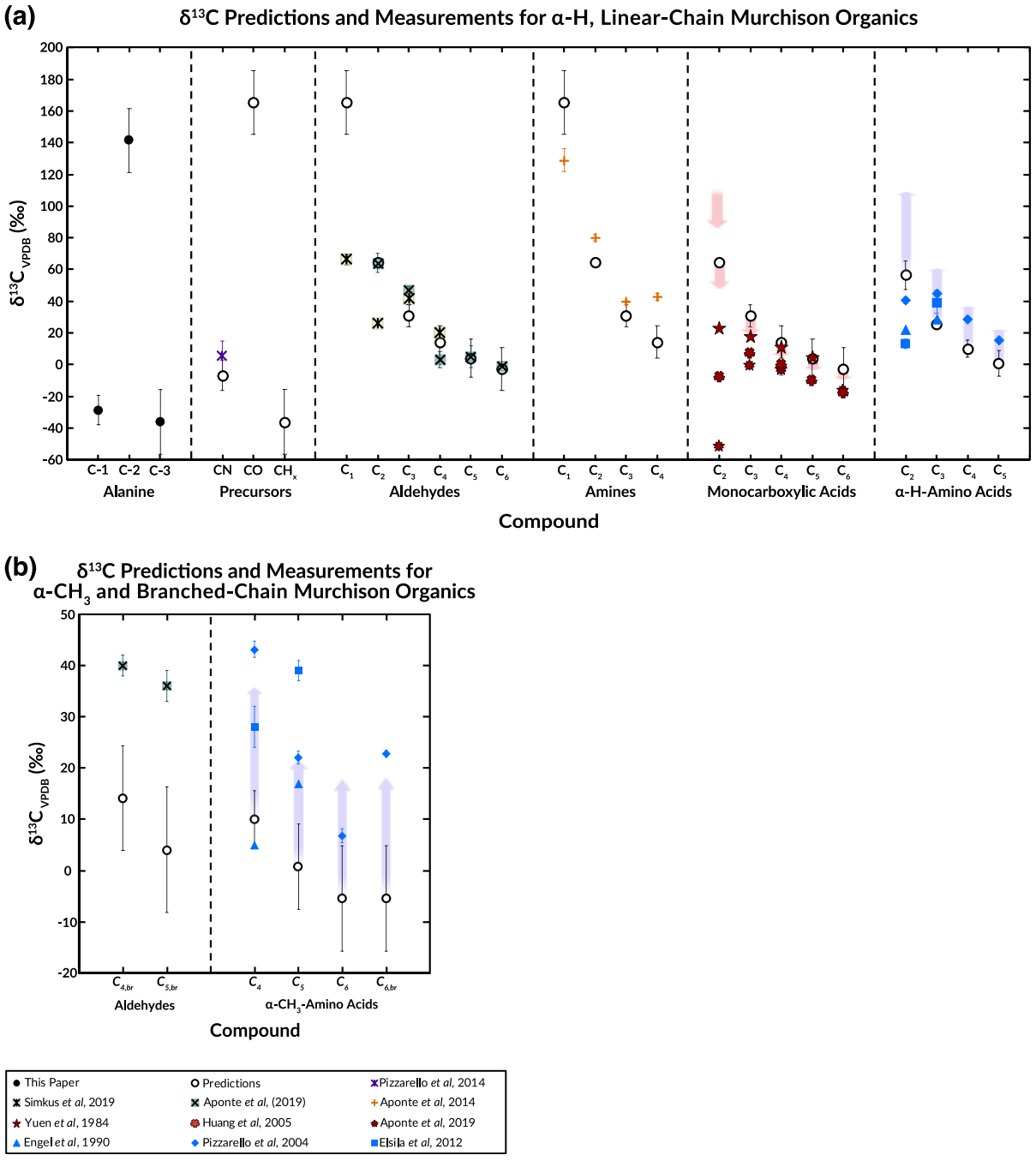

Fig. 4. (A) Comparison of $\delta^{13}C$ measurements from this study, model predictions, and literature values for each carbon site in alanine and for molecular-averages of precursors, product aldehydes, amines, monocarboxylic acids, and α-H-amino acids with linear carbon sidechains. (B) Comparison of $\delta^{13}C$ measurements from this study, model predictions, and literature values for α-CH_3-amino acids with linear carbon sidechains (denoted with no subscript) and for aldehydes and α-CH_3-amino acids with branched carbon sidechains (denoted with *br* subscript). We only include compounds with isotopic values recorded in the literature and with alpha chiral sites as well as glycine (and possible compounds made from its proposed precursor, formaldehyde) due to its biological importance. The pink arrows display the range of values predicted based on the range of KIEs for aldehyde oxidation on the reactant CO site (the terminal COOH site in monocarboxylic acids). The purple arrows highlight the expected range of values for Strecker synthesis followed by carbon isotope exchange between DIC and the C-1 sites of α-amino acids. The subscripts denote the total number of carbons in the molecule. The error bars for carboxylic acids are smaller than symbols and are not included in the data for the Engel et al. (1990) measurements as they are not provided in the 1990 paper. (For interpretation of the references to colour in this figure legend, the reader is referred to the web version of this article.)

4.3. Predictions for the $\delta^{13}C$ of other small, water soluble organics on Murchison

The preceding findings enable us to create a testable hypothesis in the form of a chemical network connecting the synthesis of alanine in Murchison and the formation of other organic compounds, including C_1 to C_6 aldehydes, amines, carboxylic acids, and other α-amino acids in the Murchison parent body (See Appendix F, Electronic Annex 2, and references (Aponte et al., 2017; Simkus et al., 2019)). Our model above predicts an acetaldehyde precursor of alanine having carbonyl and methyl groups with $\delta^{13}C$ values of $162 \pm 20‰$ and $-36 \pm 20‰$, respectively (noting that the average of these two sites is predicted with a much narrower error of ±1.5‰). The model we present presumes that alanine and the other soluble organics we consider were synthesized from a pool of precursors (H_2O, aldehydes, HCN, NH_3) that was not significantly depleted by their growth (excepting CN, which we assume underwent 10′s of % consumption by the Strecker chemistry, as in our experiments), that all reactions occurred at the same temperature, and that none of the studied compounds are residual to losses by a fractionating side-reaction. These assumptions are clearly simplifications, but generally similar models that relax these constraints (*i.e.*, allowing for variable temperature, reaction progress or side reactions) do not strongly impact our predictions (Appendix F). If formaldehyde and acetaldehyde have the same carbonyl source as expected for ISM-derived aldehyde, then the $\delta^{13}C$ of formaldehyde should be $162 \pm 20‰$. Likewise, larger aldehyde precursors would be predicted to have molecular $\delta^{13}C$ values equal to the weighted average of their one ^{13}C-rich carbonyl carbon and some additional number of ^{13}C-poor R-group carbons similar in ^{13}C isotopic composition to acetaldehyde's methyl group. These predictions agree with some molecular-average measurements of individual linear aldehydes having 2–5 carbon atoms from Murchison (Fig. 4a), but they over-predict the $\delta^{13}C$ measured for formaldehyde (Simkus et al., 2019) and under-predict the measured differences between branched and linear compounds (Fig. 4b, *refs 23* and *24*). Data from (Simkus et al., 2019) disagree with our predicted acetaldehyde value but agree with our predictions for C_4 and C_5 linear aldehydes and still display modest ^{13}C-enrichments for C_2 and C_3 linear aldehydes.

We hypothesize that other molecules with amine functional groups in Murchison were formed by reductive amination of the same aldehyde precursors that formed alanine through Strecker synthesis. Past measurements of reductive amination have demonstrated negligible KIEs of less than 1‰ (Billault et al., 2007), so the carbon backbones of other organic amines should resemble the parent aldehyde in our proposed mechanism. This hypothesis leads to $\delta^{13}C$ predictions of $162 \pm 20‰$, $62.6 \pm 1.5‰$, $30 \pm 7‰$, and $13 \pm 10‰$ for methyl-, ethyl-, propyl-, and butylamine, respectively, which resemble previous measurements from Murchison (Fig. 4 and (Aponte et al., 2016)). However, the predictions cannot account for the lack of measured difference in $\delta^{13}C$ between the C_3 and C_4 amines.

Similarly, we hypothesize that aldehyde precursors in Murchison can be oxidized into monocarboxylic acids via hydration and hydrogen abstraction at the carbonyl carbon. In the presence of water and metal oxides, aldehydes can be oxidized (Rajesh and Ozkan, 1993) to form carboxylic acids. Metal oxide catalysts are present in Murchison and other CM2 meteorites (Bunch and Olsen, 1975; Hanowski and Brearley, 2000), supporting the plausibility of this scenario. Accounting for previously measured KIEs associated with addition reactions to aldehydes (a 0 to −19‰ KIE for carbonyl carbons; (Yamataka et al., 1997; Yamataka et al., 2001)) and the likely upper limit of a ∼−30‰ KIE for the oxidation of a carbonyl carbon, the $\delta^{13}C$ values of the C_1-C_5 monocarboxylic acids can be calculated as a mixture of a ^{13}C-enriched carbonyl carbon and ^{13}C-depleted methyl carbons. The final predicted monocarboxylic acid molecular-average $\delta^{13}C$ values vary little between the 0‰ and −30‰ isotope effects on the carbonyl carbon, so we will consider the −30‰ predictions that closely agree with previous measurements for the C_3-C_5 species from Yuen et al. (1984) and with the trends presented in more recent studies by (Huang et al., 2005) and (Aponte, Woodward, et al., 2019) (Fig. 4a). The overprediction of acetic acid's $\delta^{13}C$ relative to data from all studies (Yuen et al., 1984; Huang et al., 2005; Aponte, Woodward, et al., 2019), in conjunction with the larger range of measured $\delta^{13}C$ values for acetic acid (∼75‰) versus those for other monocarboxylic acids (0–20‰) (Fig. 4a) supports the argument that the acetic acid measured on Murchison is a mixture of two or more sources (Huang et al., 2005). Furthermore, the differences in past monocarboxylic acid $\delta^{13}C$ measurements from both our predictions and from each other (Yuen et al., 1984; Huang et al., 2005; Aponte, Woodward, et al., 2019) could reflect spatial $\delta^{13}C$ heterogeneity of these components that our model does not capture as it bases its predictions on $\delta^{13}C$ values from one compound from one meteorite sample (see Appendix F). Studies of site-specific isotope ratios of monocarboxylic acids and aldehydes could provide a means of further testing and refining our understanding of the relationships amongst these compounds in Murchison as they play a critical role in the network of reactions in which amino acid synthesis occurs. Despite these complexities in the prior carbon isotope data, the relatively straightforward, unified chemical reaction network we propose provides a coherent and accurate explanation for the measured $\delta^{13}C$ values of alanine, reactant HCN, and most aldehydes, amines and monocarboxylic acids in Murchison, based only on two assumed $\delta^{13}C$ values (that for CO and CH_x precursors in the ISM; see Fig. 3 and Appendix F). The most noteworthy disagreements between our model and prior data for Murchison extracts are for formaldehyde and glycine. These are among the most volatile and easily contaminated compounds that we considered, and we suggest their high variability among prior studies and lower-than-predicted average values may reflect particularly poor preservation.

4.4. Model shortcomings

Four complicating factors prevent us from extending our model to all amino acids in Murchison that have $\delta^{13}C$ measurements: (1) prior studies yield ranges of up to 30‰ in $\delta^{13}C$ for individual amino acids (Engel et al., 1990; Pizzarello et al., 2004; Elsila et al., 2012), possibly reflecting spatial variation in precursors, reaction progress, and/or terrestrial contamination between sub-samples; (2) amino acids as a whole are structurally diverse and draw on a variety of precursors that may not have been uniform in their ^{13}C contents; (3) amino acids can be subject to side reactions not considered in the simple reaction network outlined above; and (4) Strecker synthesis can only produce α-amino acids, so all others (*e.g.*, β, γ, δ) require other synthetic routes. Nevertheless, it is straightforward to extend our hypothesis to an approximate prediction of the molecular-average $\delta^{13}C$ values of the α-amino acids. If we assume all the C-1 and C-2 sites in α-amino acids have $\delta^{13}C$ values that are identical to those observed in alanine and that all other carbon atoms have $\delta^{13}C$ values equal to that of the C-3 site in alanine (as would occur if all form by Strecker synthesis from a closely related pool of aldehyde precursors and HCN as outlined above and in Fig. 3), then we can calculate the molecular average $\delta^{13}C$ values of the other individual α-amino acids. The results are similar to most prior measurements of the C_2-C_5 α-H-amino acids, except a subset of glycine measurements; there are several possible explanations for this discrepancy, but we note that glycine is unusual in being achiral and is suspected to have been synthesized by multiple mechanisms (Fig. 4) (Engel et al., 1990; Pizzarello et al., 2004; Elsila et al., 2012).

The model presented here consistently under-predicts $\delta^{13}C$ values of both branched aldehydes and α-CH_3-amino acids (Engel et al., 1990; Pizzarello et al., 2004; Elsila et al., 2012) (Fig. 4b). One possible cause of higher measured $\delta^{13}C$ values in the amino acids, particularly the α-CH_3 amino acids, in Murchison samples is isotopic exchange between carboxyl sites and dissolved inorganic carbon (DIC) present during parent-body aqueous alteration. Theoretical calculations demonstrate that this exchange can occur for amino acids (Rustad, 2009; Pietrucci et al., 2018), has lower energy barriers for α-CH_3 species than for α-H species (Pietrucci et al., 2018), and high-$\delta^{13}C$ carbonate minerals in Murchison attest to the presence of a ^{13}C-rich DIC pool (est. with the highest measured value of +80‰ (Sephton, 2002) to present the full possible range of $\delta^{13}C$ values, see SI) during aqueous alteration. The measured molecular-average $\delta^{13}C$ values of the α-CH_3 amino acids are similar to those predicted by our model of Strecker synthesis if it is followed by equilibration of carboxyl sites with the DIC pool (purple arrows in Figs. 3 and 4). Our predictions represent a maximum $\delta^{13}C_{VPDB}$ change in the amino acids (top of the purple arrows in Fig. 4). The isotopic composition of DIC varies on Murchison samples; therefore, a lower amount of exchange and/or exchange with a less enriched $\delta^{13}C_{VPDB}$ DIC pool would result in $\delta^{13}C_{VPDB}$ values that span the length of the purple arrows in Fig. 4. It may be that partial exchange and/or lower $\delta^{13}C$ DIC pools explain why some of the α-H amino acids have $\delta^{13}C_{VPDB}$ values lower than predicted by our model. This mechanism would not function on the monocarboxylic acids without moieties on the C-2 site with a lone pair (*e.g.*, NH_2 or OH) as the C-2 site could not switch between sp^3 and sp^2 as easily. This explanation for the $\delta^{13}C$ values of the amino acids is not unique; however, it captures the full range of observations with a single plausible addition to an already parsimonious model. Branched-aldehydes and branched-sidechain amino acids require different explanations as both would require a less favorable exchange of C in saturated hydrocarbon chains. The differences in isotopic content between linear and branched compounds is another attractive target for further studies of site-specific isotopic contents of meteoritic organics.

5. CONCLUSIONS

The arguments and data presented here suggest that Strecker synthesis is likely the origin of alanine in the Murchison meteorite and that aldehydes formed from CO and CH_x in the ISM are essential precursors to a wide range of the prebiotic organic compounds observed in Murchison. These organic compounds include amino acids, amines, and carboxylic acids that formed when the ISM-sourced aldehydes reacted with HCN, NH_3, and water. Following the production of amino acids, isotopic exchange between the carboxyl group and ^{13}C-rich DIC pool might have occurred in at least some α-amino acids, approaching equilibrium for the relatively exchangeable α-CH_3 amino acids. The success of a simple reaction model (Fig. 3) in explaining most of the $\delta^{13}C$ values previously measured for these diverse compounds supports the idea that the various chemical reactions called on occurred concurrently, in a single environment, and drawing on a common pool of precursors, some of which likely originated in the ISM(de Marcellus et al., 2015). Aqueous alteration in the Murchison parent body is a plausible setting where this could have transpired.

In the future, more precise measurements of $\delta^{13}C$ values of organic compounds in the ISM will help test and refine this model by constraining initial isotope values in ISM as well as locations where these enrichments occur for different carbon pools.

Declaration of Competing Interest

The authors declare that they have no known competing financial interests or personal relationships that could have appeared to influence the work reported in this paper.

ACKNOWLEDGMENTS

We would like to acknowledge Dr. Max Klatte and Dr. Carl Blumenfeld for aiding with the Strecker synthesis of alanine. We would also like to acknowledge Thermo Fischer and Caltech for supporting the Caltech center for Isotomics.

FUNDING

This project was supported by NASA through LARS grant number NNX17AE52G and through part of the Planetary Science Division Internal Scientist Funding Program through the Fundamental Laboratory Research (FLaRe) work package of the Planetary Science Division Internal Scientist Funding Program, by The Department of Energy through DOE grant DE-SC0016561, and by the Simons Foundations;

AUTHOR CONTRIBUTIONS

LC, BD, ALS, and JME designed methods for site-specific carbon isotope measurements. JEE, JPD, and JA provided Murchison sample. JEE extracted amino acids and measured molecular-average isotope ratios of alanine. LC and JME created the Monte Carlo simulation to calculate isotope ratios. LC measured alanine on Murchison meteorite, processed data, and calculated site-specific isotope ratios. LC, JEE, JPD, JA, ALS, and JME contributed ideas to form the parent-body organic synthesis model.

DATA AND MATERIALS AVAILABILITY

All data is available in the main text or the Supplementary Information.

APPENDIX A. SUPPLEMENTARY MATERIAL

Supplementary data to this article can be found online at https://doi.org/10.1016/j.gca.2020.09.026.

REFERENCES

Aponte J. C., Dworkin J. P. and Elsila J. E. (2014) Assessing the origins of aliphatic amines in the Murchison meteorite from their compound-specific carbon isotopic ratios and enantiomeric composition. *Geochim. Cosmochim. Acta* **141**, 331–345.

Aponte J. C., Elsila J. E., Glavin D. P., Milam S. N., Charnley S. B. and Dworkin J. P. (2017) Pathways to meteoritic glycine and methylamine. *ACS Earth Space Chem.* **1**(1), 3–13.

Aponte J. C., McLain H. L., Dworkin J. P. and Elsila J. E. (2016) Aliphatic amines in Antarctic CR2, CM2, and CM1/2 carbonaceous chondrites. *Geochim. Cosmochim. Acta* **189**, 296–311.

Aponte J. C., Whitaker D., Powner M. W., Elsila J. E. and Dworkin J. P. (2019) Analyses of aliphatic aldehydes and ketones in carbonaceous chondrites. *ACS Earth Space Chem.* **3** (3), 463–472.

Aponte J. C., Woodward H. K., Abreu N. M., Elsila J. E. and Dworkin J. P. (2019) Molecular distribution,^{13}C-isotope, and enantiomeric compositions of carbonaceous chondrite monocarboxylic acids. *Meteorit. Planet. Sci.* **54**, 415–430.

Bernstein M. P., Dworkin J. P., Sandford S. A., Cooper G. W. and Allamandola L. J. (2002) Racemic amino acids from the ultraviolet photolysis of interstellar ice analogues. *Nature* **416** (6879), 401–403.

Billault I., Courant F., Pasquereau L., Derrien S., Robins R. J. and Naulet N. (2007) Correlation between the synthetic origin of methamphetamine samples and their ^{15}N and ^{13}C stable isotope ratios. *Anal. Chim. Acta* **593**, 20–29.

Botta O. and Bada J. L. (2002) Extraterrestrial organic compounds in meteorites. *Surv. Geophys.* **23**, 411–467.

Brand W. A., Assonov S. S. and Coplen T. B. (2010) Correction for the ^{17}O interference in δ^{13}C measurements when analyzing CO_2 with stable isotope mass spectrometry (IUPAC Technical Report). *Pure Appl. Chem.* **82**, 1719–1733.

Bunch T. E. and Olsen E. (1975) Distribution and significance of chromium in meteorites. *Geochim. Cosmochim. Acta* **39**, 911–927.

Burton A. S., Elsila J. E., Hein J. E., Glavin D. P. and Dworkin J. P. (2013) Extraterrestrial amino acids identified in metal-rich CH and CB carbonaceous chondrites from Antarctica. *Meteorit. Planet. Sci.* **48**, 390–402.

Burton A. S., Stern J. C., Elsila J. E., Glavin D. P. and Dworkin J. P. (2012) Understanding prebiotic chemistry through the analysis of extraterrestrial amino acids and nucleobases in meteorites. *Chem. Soc. Rev.* **41**, 5459–5472.

Charnley S. B., Ehrenfreund P., Millar T. J., Boogert A. C. A., Markwick A. J., Butner H. M., Ruiterkamp R. and Rodgers S. D. (2004) Observational tests for grain chemistry: posterior isotopic labelling. *Mon. Not. R. Astron. Soc.* **347**, 157–162.

Cooper G., Reed C., Nguyen D., Carter M. and Wang Y. (2011) Detection and formation scenario of citric acid, pyruvic acid, and other possible metabolism precursors in carbonaceous meteorites. *Proc. Natl. Acad. Sci.* **108**(34), 14015–14020.

Cordiner M. A., Palmer M. Y., de Val-Borro M., Charnley S. B., Paganini L., Villanueva G., Bockelée-Morvan D., Biver N., Remijan A. J., Kuan Y. J., Milam S. N., Crovisier J., Lis D. C. and Mumma M. J. (2019) ALMA autocorrelation spectroscopy of comets: the HCN/H13CN ratio in C/2012 S1 (ISON). *Astrophysi J.* **870**, L26.

Cronin J. R., Cooper G. W. and Pizzarello S. (1995) Characteristics and formation of amino acids and hydroxy acids of the Murchison meteorite. *Adv. Space Res.* **15**(3), 91–97.

Cronin J. R. and Moore C. B. (1971) Amino acid analyses of the murchison, murray, and allende carbonaceous chondrites. *Science* **172**(3990), 1327–1329.

Eiler J., Cesar J., Chimiak L., Dallas B., Grice K., Griep-Raming J., Juchelka D., Kitchen N., Lloyd M., Makarov A., Robins R. and Schwieters J. (2017) Analysis of molecular isotopic structures at high precision and accuracy by Orbitrap mass spectrometry. *Int. J. Mass Spectrom.* **422**, 126–142.

Eisenhauer F., Schdel R., Genzel R., Ott T., Tecza M., Abuter R., Eckart A. and Alexander T. (2003) A geometric determination of the distance to the galactic center. *ApJ* **597**(2), L121–L124.

Elsila J. E., Aponte J. C., Blackmond D. G., Burton A. S., Dworkin J. P. and Glavin D. P. (2016) Meteoritic amino acids: diversity in compositions reflects parent body histories. *ACS Cent. Sci.* **2**, 370–379.

Elsila J. E., Charnley S. B., Burton A. S., Glavin D. P. and Dworkin J. P. (2012) Compound-specific carbon, nitrogen, and hydrogen isotopic ratios for amino acids in CM and CR chondrites and their use in evaluating potential formation pathways. *Meteorit. Planet. Sci.* **47**, 1517–1536.

Elsila J. E., Dworkin J. P., Bernstein M. P., Martin M. P. and Sandford S. A. (2007) Mechanisms of amino acid formation in interstellar ice analogs. *Astrophys. J.* **660**, 911–918.

Engel M. H., Macko S. A. and Silfer J. A. (1990) Carbon isotope composition of individual amino acids in the Murchison meteorite. *Nature* **348**(6296), 47–49.

Friedrich J. M., McLain H. L., Dworkin J. P., Glavin D. P., Towbin W. H., Hill M. and Ebel D. S. (2018) Effect of polychromatic X-ray microtomography imaging on the amino

acid content of the Murchison CM chondrite. *Meteorit. Planet Sci.* **54**(1), 220–228.

Glavin D. P., Alexander C. M. O., Aponte J. C., Dworkin J. P., Elsila J. E. and Yabuta H. (2018) The origin and evolution of organic matter in carbonaceous chondrites and links to their parent bodies. In Primitive Meteorites and Asteroids. Elsevier. pp. 205–271.

Glavin D. P., Callahan M. P., Dworkin J. P. and Elsila J. E. (2010) The effects of parent body processes on amino acids in carbonaceous chondrites. *Meteorit. Planet. Sci.* **45**, 1948–1972.

Hanowski N. P. and Brearley A. J. (2000) Iron-rich aureoles in the CM carbonaceous chondrites Murray, Murchison, and Allan Hills 81002: Evidence for*in situ* aqueous alteration. *Meteorit. Planet. Sci.* **35**, 1291–1308.

Hoffman D. W. and Rasmussen C. (2019) Position-specific carbon stable isotope ratios by proton NMR spectroscopy. *Anal. Chem.* **91**, 15661–15669.

Huang Y., Wang Y., Alexandre M. R., Lee T., Rose-Petruck C., Fuller M. and Pizzarello S. (2005) Molecular and compound-specific isotopic characterization of monocarboxylic acids in carbonaceous meteorites. *Geochim. Cosmochim. Acta* **69**, 1073–1084.

Kerridge J. F. (1999) Formation and processing of organics in the early solar system. *Space Sci. Rev.* **90**, 275–288.

Lallement R., Capitanio L., Ruiz-Dern L., Danielski C., Babusiaux C., Vergely L., Elyajouri M., Arenou F. and Leclerc N. (2018) Three-dimensional maps of interstellar dust in the Local Arm: using *Gai*a, 2MASS, and APOGEE-DR14. *A&A* **616**, A132.

Langer W. D., Graedel T. E., Frerking M. A. and Armentrout P. B. (1984) Carbon and oxygen isotope fractionation in dense interstellar clouds. *Astrophys. J.* **277**, 581–590.

Langer W. D. and Penzias A. A. (1990) C-12/C-13 isotope ratio across the Galaxy from observations of $^{13}C/^{18}O$ in molecular clouds. *Astrophys. J.* **357**, 477–492.

Lynn K. R. and Yankwich P. E. (1961) Cyanide carbon isotope fractionation in the reaction of cyanide ion and methyl iodide. carbon isotope effect in the hydrolysis of methyl iodide. *J. Am. Chem. Soc.* **83**(1), 53–57.

Lyons J. R., Gharib-Nezhad E. and Ayres T. R. (2018) A light carbon isotope composition for the Sun. *Nat. Commun.* **9**, 908.

de Marcellus P., Meinert C., Myrgorodska I., Nahon L., Buhse T., d'Hendecourt L. L. S. and Meierhenrich U. J. (2015) Aldehydes and sugars from evolved precometary ice analogs: importance of ices in astrochemical and prebiotic evolution. *Proc. Natl. Acad. Sci. USA* **112**(4), 965–970.

Martins Z. and Sephton M. A. (2009) Extraterrestrial amino acids. In Amino acids, peptides and proteins in organic chemistry: origins and synthesis of amino acids (ed. A. B. Hughes). Wiley-VCH Verlag GmbH & Co. KGaA, Weinheim, Germany. pp. 1–42.

Mccollom T. and Seewald J. (2006) Carbon isotope composition of organic compounds produced by abiotic synthesis under hydrothermal conditions. *Earth Planet. Sci. Lett.* **243**, 74–84.

Merritt D. A. and Hayes J. M. (1994) Factors controlling precision and accuracy in isotope-ratio-monitoring mass spectrometry. *Anal. Chem.* **66**, 2336–2347.

Milam S. N., Savage C., Brewster M. A., Ziurys L. M. and Wyckoff S. (2005) The $^{12}C/^{13}C$ isotope gradient derived from millimeter transitions of CN: The case for galactic chemical evolution. *Astrophys. J.* **634**, 1126.

Pietrucci F., Aponte J. C., Starr R., Pérez-Villa A., Elsila J. E., Dworkin J. P. and Saitta A. M. (2018) Hydrothermal decomposition of amino acids and origins of prebiotic meteoritic organic compounds. *ACS Earth Space Chem.* **2** (6), 588–598.

Pizzarello S. (2014) The nitrogen isotopic composition of meteoritic HCN. *Astrophys. J.* **796**, L25.

Pizzarello S., Cooper G. W. and Flynn G. J. (2006) The nature and distribution of the organic material in carbonaceous chondrites and interplanetary dust particles. *Meteorites Early Sol. Syst. II* **1**, 625–651.

Pizzarello S., Huang Y. and Fuller M. (2004) The carbon isotopic distribution of Murchison amino acids. *Geochim. Cosmochim. Acta* **68**, 4963–4969.

Pizzarello S., Krishnamurthy R. V., Epstein S. and Cronin J. R. (1991) Isotopic analyses of amino acids from the Murchison meteorite. *Geochim. Cosmochim. Acta* **55**, 905–910.

Rajesh H. and Ozkan U. S. (1993) Complete oxidation of ethanol, acetaldehyde and ethanol/methanol mixtures over copper oxide and copper-chromium oxide catalysts. *Ind. Eng. Chem. Res.* **32**, 1622–1630.

Rustad J. R. (2009) Ab initio calculation of the carbon isotope signatures of amino acids. *Org. Geochem.* **40**(6), 720–723.

Sephton M. A. (2002) Organic compounds in carbonaceous meteorites. *Nat. Prod. Rep.* **19**, 292–311.

Simkus D. N., Aponte J. C., Hilts R. W., Elsila J. E. and Herd C. D. K. (2019) Compound-specific carbon isotope compositions of aldehydes and ketones in the Murchison meteorite. *Meteorit. Planet. Sci.* **54**, 142–156.

Taran Y. A., Kliger G. A. and Sevastianov V. S. (2007) Carbon isotope effects in the open-system Fischer-Tropsch synthesis. *Geochim. Cosmochim. Acta* **71**, 4474–4487.

Van Trump J. E. (1975) *The Strecker synthesis and its prebiological importance* Doctoral dissertation. University of California, San Diego.

Yamataka H., Sasaki D., Kuwatani Y., Mishima M., Shimizu M. and Tsuno Y. (2001) Reactions of PhSCH(2)Li and NCCH(2) Li with benzaldehyde and benzophenone: when does the mechanism change from ET to polar? *J. Org. Chem.* **66**, 2131–2135.

Yamataka H., Sasaki D., Kuwatani Y., Mishima M. and Tsuno Y. (1997) On the mechanism of addition of lithium pinacolone enolate to benzaldehyde: polar or electron transfer? *J. Am. Chem. Soc.* **119**, 9975–9979.

Yuen G., Blair N., Des Marais D. J. and Chang S. (1984) Carbon isotope composition of low molecular weight hydrocarbons and monocarboxylic acids from Murchison meteorite. *Nature* **307** (5948), 252–254.

Associate editor: Eric Quirico

Appendix A: Calibration of alanine standards for Site-Specific Isotope Ratio (SSIR) Measurements

The molecular-average $\delta^{13}C$ values of pure alanine standards were measured on a Thermo Fisher Scientific Flash Elemental Analyzer (EA) coupled to a Delta-V isotope ratio mass spectrometer (IRMS) at Caltech. Alanine standards are described above (See Materials: Derivatization). A lab acetanilide standard served as check on accuracy of $\delta^{13}C$ measurements. The $\delta^{13}C$ values and associated uncertainties for the alanine standards are -19.4 ± 0.1 ‰, -20.0 ± 0.2 ‰, and -32.9 ± 0.2 ‰ for Alfa Aesar, VWR, and Strecker alanine respectively (Eiler et al., 2017) (Table 1); acetanilide was measured to have a $\delta^{13}C$ value of -27.6 ± 0.1 ‰ in good agreement with its prior measured value of -27.7 ± 1.7‰.

The Alfa Aesar and Strecker alanine standards were also analyzed at GSFC following protocols from (Elsila et al., 2012) using coupled GC-combustion-IRMS (GC-C-IRMS), which enables isotopic analysis of individual amino acids in mixtures such as those from the Murchison extracts. After accounting for dilution effects from the derivative methyl and isopropyl groups (See Data Processing and (Elsila et al., 2012) for details on dilution effects), the standards' $\delta^{13}C$ values were -19.4 ± 0.2 ‰ and -33.3 ± 0.1 ‰ for Alfa Aesar and Strecker respectively, which is within two standard errors of those measured at Caltech (Table 1).

We also measured the $\delta^{13}C$ values of C-1 in all 3 alanine standards via ninhydrin decarboxylation, following methods from (Van Slyke et al., 1941) and (Abelson and Hoering, 1961). Resulting $\delta^{13}C_{VPDB}$ values for C-1 were -28.5 ± 0.1 ‰, -29.5 ± 0.3 ‰, -43.5 ± 0.1 ‰, for the Alfa Aesar, VWR, and Strecker standards, respectively (Eiler et al., 2017). Combining these

data with the molecular-average $\delta^{13}C$ values from above allowed us to calculate the average $\delta^{13}C$ of their combined C-2 and C-3 sites (See Section 2.3: Data Processing for calculations and Figure 1a in main text for alanine with labelled carbon sites) as -14.8 ± 0.6 ‰, -27.6 ± 0.3 ‰, and -15.6 ± 0.3 ‰. At the time of this publication, we have no independent evidence regarding the individual isotopic compositions of the C-2 and C-3 sites in these standards; however, NMR studies of site-specific carbon isotope ratios of amino acids (R. Robins pers. com.) indicate that all common terrestrial forms of these amino acids, including standards purchased from Sigma Aldrich (BioUltra, >99% Purity, Lot# BCBM6312V), have $\delta^{13}C_{VPDB}$ fractionations between C-2 and C-3 in each molecule that are 10 ‰ or less, which is in the upper range of differences between methyl and adjacent cites for other small organics (Gilbert et al., 2011). The differences we observe in the Murchison sample relative to the Alfa Aesar standard C-2 and C-3 are on the order of 170 ‰, and the error of the C-3 calculation (10 ‰) is within error of the 10 ‰ difference found between C-2 and C-3 in other alanine samples. Consequently, the potential 10 ‰ difference is negligible in our study, and for this study we assume our standards have C-2 and C-3 sites that are identical in $\delta^{13}C$. Future measurements of one or more of the standards used in this study could be used to refine the data presented here in order to account for the likely small differences between C-2 and C-3 in our alanine standards, but we think it implausible that our conclusions could be influenced by the small isotopic differences between these sites likely present in our terrestrial standards.

Site-specific $\delta^{13}C$ values for the Methods Development samples measured in December and March are within error of one another (Table 1). We interpret the differences in site-specific isotope ratios between methods development and analytical samples as being due to terrestrial contamination (though it is also possible that they partially reflect differences in isotopic

composition between the alanine native to these two Murchison samples or fractionations arising from chemical reactions of sample alanine during storage). Regardless, we base our discussion of the Murchison sample only on the analytical sample. We present the data for the methods development sample only in order to document the development of the methods used in this study.

Appendix B: Blanks

Multiple procedural blanks were carried through the workup and analyzed alongside the Methods Development and Analytical samples. All blanks start at their listed step (*e.g.*, extraction, transfer, derivatization; see Table S1) and follow all subsequent steps through derivatization as outlined in Figure S2. As an example, blanks designed to test the extraction of amino acids had water added to an empty ampoule after which all subsequent extraction, transfer, and derivatization steps were followed. Thus, all blanks should only contain derivatizing reagents, the products of their reactions with one another, and hexane if sample processing produced no contamination. Procedural Blanks are summarized in Table S1 and consisted of the following: (1a and 1b) blanks that tested reagents used in the derivatization of alanine (our ultimate analytical target), (2) a blank that starts with water leaching at GSFC and continues through chemical derivatization at Caltech, (3) a blank that starts with the water:methanol transfer of the meteorite extract into a GC vial at Caltech, and (4) a blank that starts with analyte derivatization at Caltech (See Figure S2). Procedural Blanks 1a and 1b occurred prior to the day of meteorite extract derivatization while Procedural Blanks 2-4 occurred on the same day as the corresponding meteorite extract derivatization. Additional solvent blanks (injections of hexane

into the Orbitrap) and instrument blanks (temperature ramps with no injection) were run prior to each meteorite analysis to test the instrument background.

Each procedural blank was analyzed in Direct Injection mode on the Orbitrap, and signals were integrated between 6.5 and 8.5 minutes after injection for ^{12}C and ^{13}C counts from *m/z* 140.032 and 141.035 fragment peaks (for conversion from signal intensity to counts see(Eiler et al., 2017). Alanine elutes at ~7.5 minutes and is typically transferred into the reservoir from approximately 7–8 minutes retention time, so counting the background over 2 minutes overestimates possible contamination. As with the sample data (see Site-Specific Isotope Analysis and Data Processing) data used to calculate ^{13}R was culled only to include scans that contained both the monoisotopic and singly ^{13}C-substituted fragment and was computed using a counts-weighted average of all ^{13}R values in the blank. Reported sums of ^{12}C and ^{13}C counts (Dataset S1) use all scans including those which have only the monoisotopic or the singly ^{13}C substituted fragment without the other in order demonstrate the maximum possible error in our measurements. When compared to samples measured with the Reservoir Elution mode, the overestimation is even greater because in Reservoir Elution mode measurements are broadened over many tens of minutes, giving them a lower signal-to-noise ratio (which is inversely proportional to counts reported). The procedural blank for analytical Murchison that had the highest amount of contamination in all metrics was Procedural Blank 2 (Table S1), which started with the meteorite extraction at GSFC. However, compared to the 15 pmol/μL alanine in the analytical sample, Procedural Blank 2 contained 0.15 pmol/μL and could account for only 1.9 % of the integrated ^{12}C counts, 0.7% of the integrated ^{13}C counts, and 0.3 % of the integrated ^{12}C signal intensity relative to the directly injected Murchison sample. The 140.032 and 141.035 *m/z*

fragments are the most abundant ones in the mass spectrum of alanine. Maximum abundances of *m/z* 140.032 and 141.035 ions in blanks were low (see Dataset S1) and did not appear during the 7.41-7.73 window during which alanine elutes, so these background signals likely either represent other compounds derived from column bleed, reagents, etc., and/or part of the instrument background. For chromatograms and spectra of blanks and Murchison, see Figure S3.

Solvent blanks and instrument blanks were run prior to meteorite sample analyses and also processed for integrated ^{12}C and ^{13}C counts from 6.5 to 8.5 minutes elution time (Table S2). These measurements find background ^{12}C and ^{13}C counts arising from the injector, column, transfer lines, etc. to typically account for less than 0.5% of the measured ^{12}C and ^{13}C counts in Murchison samples and a <0.05 ‰ change in ^{13}R values. Of the fragments used to calculate the site-specific isotope ratios of alanine, the highest background signals were observed for the *m/z* 184.021 fragment. In this case, the background counts account for approximately 0.5 % of the measured signal but change the ^{13}R value by only ~0.03 ‰, which is well within the ~10 ‰ standard error of the measurements at the 184.021 fragment. The low procedural blanks and instrument background demonstrate that our ^{13}R values reflect alanine from the meteorite rather than background or contamination.

Appendix C: Potential additional constraints for alanine SSIR measurement

We attempted to add a fourth constraint to our characterization of the carbon isotope structure of alanine by measuring the ^{13}R of a fragment ion having a monoisotopic mass of 113.0208 ($C_3H_4OF_3$). The straightforward fragment suggested by this mass would be $CF_3CH(O)CH_3$ using C-2 from the parent alanine. However, our studies of labeled alanines suggest that this fragment

only receives sample carbon atoms from C-3 of the parent alanine along with two carbons from the TFAA derivatizing reagents and none from C-2 of the parent alanine. The stoichiometry of this ion suggests it is a recombination product (*i.e.*, because direct fragmentation of the parent molecule cannot create a single piece containing these sites). We infer C-3 of alanine recombines with COH and CF_3 from the TFAA derivatizing reagent either as a two-body reaction or as two stepwise reactions. This complexity calls into question whether such a measurement could yield a consistent constraint on the ^{13}R of C-3 because the yields of recombination reactions generally depend on source pressure and other analytical variables (*i.e.*, we can imagine the same ion might be produced through other pathways when analytical conditions are varied). In any case, when we attempted to apply this method to the derivatized Murchison extract our peak captures of alanine were contaminated by at least one subsequent peak of a different compound. We recognize one such candidate contaminant peak also produces a 113.0208 Da fragment ion. Thus, we consider these measurements to have failed for reasons having to do with our chromatographic separations and peak trapping. We report these results in the for completeness, but we do not use these data as constraints on the Murchison sample carbon isotope structure.

Appendix D: Error Analysis

Errors for the Total Orbitrap and the Combined Orbitrap/GC-C-MS calculations were weighted according to the proportion effect of their value on the final calculation and then added in quadrature (Eqn. A1a-A1c):

Combined Orbitrap(140,184)/GC-C-IRMS Calculation Error

$$^{13}\sigma_{C\text{-}1} = \{(3 \times {}^{13}\sigma_{molec\ avg})^2 + (2 \times {}^{13}\sigma_{C\text{-}2+C\text{-}3})^2\}^{0.5} \qquad (A1a)$$

$$^{13}\sigma_{C\text{-}2} = \{(2 \times {}^{13}\sigma_{C\text{-}1+C\text{-}2})^2 + {}^{13}\sigma_{C\text{-}1}{}^2\}^{0.5} \quad (A1b)$$

$$^{13}\sigma_{C\text{-}3} = \{(2 \times {}^{13}\sigma_{C\text{-}2+C\text{-}3})^2 + {}^{13}\sigma_{C\text{-}2}{}^2\}^{0.5} \quad (A1c)$$

It is important to note that the resulting computed errors for the three alanine sites are highly correlated with one another due to interdependencies among the functions that relate them to the various measured ratios. In particular, the $\delta^{13}C$ of C-2 and C-3 are associated with large errors, yet their average is known to within 1.5 ‰ (1SE). The primary control on the error is the experimental uncertainty in the average C-1 + C-2 $\delta^{13}C$, which is doubled in computing the site-specific uncertainty of the C-2 site (See Eqn. A1b) and then propagated into the calculated $\delta^{13}C$ of the C-3 site. If future studies improve in the precision of the results presented here, it will be productive to focus on these dependencies; in particular, a highly precise molecular-average measurement that includes the derivative carbons, a high precision analysis of the *m/z* = 184.021, and a high precision analysis of the fragment *m/z* = 113.032 fragment with peak capturing that excludes subsequent peaks. These improvements were not possible during this study due to limited sample sizes, but a more ambitious effort to extract and purify alanine from Murchison might achieve errors on the order of ~1 ‰ for all sites (see (Neubauer et al., 2018) for an example of high precision amino acid C isotope structures measured using our techniques).

Appendix E: Alternative Pathways for Alanine Synthesis

In addition to acetaldehyde and cyanide reacting via Strecker synthesis, the alanine carbon isotope structure could be explained by the reductive amination of pyruvic acid(Rustad, 2009; Robins et al., 2015). In this case, the pyruvic acid would form from a ketene (ethenone) which sources its alkyl group (C-2) from the same ^{13}C-deplete CH_x pool and its CO (C-1) from the

same ^{13}C-enriched CO pool described in the main text (See Figure S4). The ethenone would then react with CN and water to form pyruvic acid that could react with NH_3 on later to form alanine. Consequently, assuming a low ^{13}C ISM CN pool, this reaction network could explain our results. Furthermore, as the reaction network (Figure S4) still involves the addition of CN to an sp^2-hybridized carbon and the oxidation of a nitrile to a carboxyl group (Rustad, 2009), the isotope effect and thus predicted initial carbon values should not greatly change between the scenarios (excepting possible changes in isotope effect due to physiochemical conditions).

Unlike the Strecker model, the pyruvate model would not provide clear pathways to amines, aldehydes, or monocarboxylic acids. Furthermore, measured values of keto acids are, as of yet, unavailable such that we could not compare predictions of this model to our data. For this reason, we chose to focus on the Strecker synthesis possibility. The agreement between our predictions and measured values across a wide range of compound classes supports the possibility that Strecker synthesis of aldehydes and cyanohydrins produced alanine and other organic compounds.

We also considered whether Murchison alanine could be the product of a reaction network in which alanine carboxyl is derived from high $\delta^{13}C$ HCN, through Strecker chemistry. This hypothesis could be indirectly supported by the observation that monocarboxylic acids in Murchison have high molecular average $\delta^{13}C$ values (Yuen et al., 1984). If these carboxylic acids formed by hydrolysis of nitriles, then those nitriles presumably could have been high in $\delta^{13}C$. And if that ^{13}C enrichment were hosted by the terminal CN group, we should expect co-existing HCN would be ^{13}C enriched. We are not aware of measurements of $\delta^{13}C$ of Murchison

nitriles (and their terminal CN groups are certainly not known). But if their terminal CN groups were enriched enough to account for the 10's of per mil enrichment of carboxylic acids, it would imply a $\delta^{13}C$ value for that group of +100 ‰ or more. This hypothesis is speculative but based on sound chemical principles and so worth considering. Nevertheless, it is strongly contradicted by data (both from previous studies and our study), so we think it must be rejected. Most simply, HCN from Murchison is relatively low in $\delta^{13}C$ (Pizzarello, 2014), and our measurement of alanine carboxyl indicates it is consistent with derivation by Strecker reaction from that measured HCN. We conclude the most parsimonious interpretation is that alanine in fact did form from the HCN present in Murchison, and that this HCN was not derived from a strongly ^{13}C-enriched pre-solar pool.

Finally, we consider the IOM as source of organics. (Huang et al., 2007) argue that monocarboxylic acids and other small organics could be produced by the hydrothermal processing of IOM. Observations that might be taken as evidence of this idea include: 1) Correlations of the $\delta^{13}C$ values of monocarboxylic acids with their carbon numbers are similar to those for moieties from the IOM; and 2) our measurements demonstrate that the IOM has an isotopic composition similar to the ^{13}C pool that was the source of the C-1 and C-3 sites of alanine, perhaps suggesting alanine is also formed by hydrolysis of IOM. This second observation could be understood in the context of the model we present if the IOM and alanine's C-1 and C-3 sites both derive from a primordial low ^{13}C pool (*i.e.*, hydrocarbons and HCN). If, instead, alanine was made from hydrolysis of the IOM, it is not obvious how it would have acquired such an extraordinarily high $\delta^{13}C$ value in its C2 carbon site without evidence of enrichment in the C1 and C3 sites. We are aware of no high ^{13}C chemical moieties of the IOM

that could readily explain this finding, and so we believe this idea could not be developed to provide a satisfactory explanation of this study's results.

Nevertheless, future compound- and site-specific measures may be able to identify IOM processing as a source of soluble organics in Murchison (and perhaps other carbonaceous chondrites). The site-specific $\delta^{13}C$ isotope ratio for compounds produced by IOM processing should mirror those found in the IOM aliphatic side chains (which have compound specific molecular average $\delta^{13}C$ values of 57.9 ‰ to 0.4 ‰). In contrast, the reaction network we propose predicts that the terminal carboxyl (C-1) sites of the carboxylic acids will be highly ^{13}C enriched compared to all other CH_x sites.

Appendix F: Parent-Body Organic Reaction Model

Constraints on the Isotope Effects Associated with Syntheses

To calculate the $\delta^{13}C$ values of alanine precursors and organic synthesis products other than alanine, isotope effects of different synthetic steps were collated from literature review and those for Strecker synthesis were measured via experimental work conducted as part of this study. Isotope effects for Strecker synthesis were further validated by comparison to literature values for isotope effects from similar reaction mechanisms.

The reduction of aldehydes into imines via reductive amination has a maximum measured isotope effect of 0.6 ‰ (Billault et al., 2007), which is lower than our measurement errors so was treated as a 0 ‰ fractionation in the model. Studies for carbon isotope effects during the oxidation of aldehydes have observed a range of effects from negligible (aldehyde to

thiohemiacetal conversion) (Canellas and Cleland, 1991) to large deuterium isotope effects that suggest possible concurrent carbon isotope effects (Wiberg, 1954); although these have not been measured. To consider both possibilities, we consider two endmember cases of 1) no isotope effect and 2) a 30‰ normal kinetic isotope effect, similar to intrinsic KIE's associated with other carbon oxidation reactions (Cleland, 2005). Mechanisms and associated isotope effects are portrayed in Figure 3 in the main text. Differences in our solution between the 0 ‰ carbonyl oxidation KIE and the 30 ‰ normal KIE case are depicted in Figure 4 in the main text.

Experimental work was conducted to constrain the isotope effects in Strecker synthesized alanine from ammonium chloride, acetaldehyde, sodium cyanide, and water at temperatures ranging from 20°C to 25°C for the creation of the aminonitrile and 80°C to 120°C for its acid hydrolysis. We measured the average isotopic composition of solid reagents and products via EA-IRMS, of acetaldehyde via combustion over CuO into CO_2 which was measured on a dual-inlet IRMS, and the site-specific isotopic composition of alanine produced by the synthesis was measured for $\delta^{13}C$ of the C-2 + C-3 (140.032 fragment) on the Orbitrap as described above. Our measurements indicated that the average $\delta^{13}C$ of C-2 and C-3 of alanine produced by Strecker synthesis (-30.6 ± 0.9 ‰) is approximately 12‰ depleted in ^{13}C relative to the reactant acetaldehyde ($\delta^{13}C$ = -19.1 ‰) regardless of yield. Because C-3 does not participate in the Strecker reaction, we assumed the difference in the average $\delta^{13}C$ for C-2 and C-3 is due to a -24 ‰ isotope effect on C-2, which is consistent with other CN addition reactions (Lynn and Yankwich, 1961). C-1 (found by a subtraction of C-2 and C-3 from the molecular average) exhibited a normal KIE that had an average value of 22 ‰ for alanine produced between a 10 % and 55 % yield

(-54.1 ± 3.2 ‰ relative to a starting CN $\delta^{13}C$ of -31.8 ± 0.2 ‰). This KIE also agrees with literature values for amide oxidation (Robins et al., 2015).

Our reaction network model assumes a low yield of products and unlimited supply of reactants relative to the products such that isotope effects would be apparent in products and but would not significantly alter the $\delta^{13}C$ of the reactants (and, consequently, other compounds produced from them). The agreement between our predicted isotope ratios and measurements in literature, particularly for acetaldehyde and HCN, is consistent with this assumption. However, below we analyze the possibility that variations in certain factors would impact our results:

Temperature: The isotope effects associated with reactions in our hypothesized reaction network range up to 30 ‰. Given that the temperatures of aqueous alteration of the CM chondrites have been demonstrated to have varied between 20 and 71 ˚C (293.15 – 344.15 K (Guo and Eiler, 2007)) through clumped isotope thermometry, and given that chemical isotope effects commonly exhibit approximately linear variations in amplitude with $1/T^2$, we estimate that these model estimates could have varied by several per mil. For moderate variations in reaction progress (below), these should lead to variations of just a few per mil in predicted $\delta^{13}C$ values of products. This is comparable to full procedural analytical precision and less than otherwise unexplained variability in the data, and so we consider it insignificant (in the context of the constraints and goals of our model).

Reaction progress: Our model presumes that essential reactants (water, aldehydes, ammonia and HCN) are more abundant than products that are created in our reaction network. If the

proportions of these compounds in the Murchison parent body initially resembled those in comets (*e.g.*, Biver *et al.*, (2019)), this assumption would be well justified. However, if organic synthesis reactions such as the Strecker chemistry locally went to near completion (consuming most of reactants), isotope effects associated with synthesis reactions would be mitigated, as isotopic proportions in products would approach those of reactants. The largest kinetic isotope effects associated with our reaction network model (30 ‰) could be diminished in this way — in the extreme limit of quantitative yield, reduced to nothing.

The limits one should place on this argument are difficult to evaluate because all of the reactants are more volatile than the products (*e.g.*, alanine is essentially involatile whereas its proposed substrates, acetaldehyde and HCN have boiling points of 20 and 26˚C, respectively). Thus, the abundance ratios of aldehydes to amino acids in the Murchison meteorite are likely a poor guide to their proportions early in the history of the Murchison parent body. If the synthesis chemistry had yields comparable to laboratory Strecker synthesis (10's of %), then the effective KIE's would be approximately halved, or reduced by approximately 10 ‰. That would be degrade the level of agreement between our model prediction and the measured $\delta^{13}C$ of some compounds in our model (and improve the level of agreement for others), but by amounts that are a small fraction of the isotopic variations (*i.e.*, site-specific and intermolecular differences) that motivate our model. We therefore consider it implausible that this factor significantly impacts the overall reasonableness of our model.

Alanine destruction: Free and total alanine in Murchison are about one-third as abundant as in the most alanine-rich CM chondrite (~0.20 and ~0.65 ppm, respectively), implying that it could

be residual to 10's of % destruction. If this destruction was accompanied by a ^{13}C kinetic isotope effect in the range typical of irreversible organic reactions (~10-30 ‰) and operated on one or two atomic sites, then the residual alanine could have been enriched in $\delta^{13}C$ by several per mil up to perhaps 10 ‰. The most likely mechanisms for alanine destruction (NH_2 replacement with OH, or decarboxylation) should either enrich the C-2 site or enrich both the C-1 and C-2 sites equally in the residue. These effects are less than or just at the margin of the level of significance addressed by our model and are a small fraction of the 150 ‰ site-specific effect our model was tailored to describe. Moreover, the $\delta^{13}C$ values of alanine from CM chondrites do not exhibit an inverse concentration with their concentration in the samples, so there is no empirical evidence to suggest such a fractionating loss mechanism. We conclude loss of alanine through these side reactions is unlikely to significantly impact our conclusions.

Calculation of reactant $\delta^{13}C$ values

To estimate the site-specific $\delta^{13}C$ values of reactants in our network model, we subtracted site-specific isotope effects constrained by our Strecker synthesis experiments from the measured $\delta^{13}C$ values for alanine in the analytical Murchison sample. Based on these results, the reactant CN is estimated to have a $\delta^{13}C_{VPDB}$ value of -7 ‰ and the initial acetaldehyde is estimated to have $\delta^{13}C_{VPDB}$ values of 166 ± 10‰ and -36 ± 10 ‰ for the carbonyl ($C\text{-}1_{acetaldehyde}$) and methyl ($C\text{-}2_{acetaldehyde}$) carbons, respectively. Combining our results with the ISM chemical networks described in (Elsila et al., 2012) and references therein, we predict that the carbonyl carbon in all aldehyde functional groups are from the ^{13}C-enriched CO pool in the ISM and that all alkyl carbons are from another, ^{13}C-depleted pool (that include C_xH_y compounds). Thus, in our model we assigned $\delta^{13}C$ values of 166 ± 10 ‰ to all carbonyl carbons and -36 ± 10 ‰ to all alkyl

carbons. Equivalently, we calculated the molecular-average $\delta^{13}C$ values of aliphatic aldehydes with two or more carbons by calculating the carbon-weighted average values of acetaldehyde (64.6 ± 1.5 ‰) and additional aliphatic carbons (-36 ± 10 ‰) (Eqn. A2; See Appendix C).

$$^{13}F_{Cx\text{-}aldehyde} = \left(\frac{2}{x}\right)^{13}F_{molec\ avg,\ acetaldehyde} + \left(\frac{x-2}{x}\right)^{13}F_{C\text{-}2,\ acetaldehyde} \qquad \textit{(Eqn. A2)}$$

where x is the carbon chain length and C_x-aldehyde is a molecule with one aldehyde carbon and x methylene carbons. All such calculations are made using ^{13}C mole fraction ("fractional abundance") rather than $\delta^{13}C$ values to avoid systematic errors arising from non-linearities of the δ scale.

In our model, amines form from a reactant aldehyde's reductive amination (Figure 3, main text), which is proposed to have an insignificant KIE, so we estimated that the $\delta^{13}C$ value of the amine molecule is equal to that of an aldehyde molecule with the same carbon backbone (See Dataset S2). Monocarboxylic acids formed from the oxidation of aldehyde precursors were assigned to have isotope effects that range from 0 ‰ to -30 ‰. In the first case, the product carboxylic acids have $\delta^{13}C$ values equal to their aldehyde precursors (See Dataset S2). For the alternate case of a fully expressed -30 ‰ KIE during oxidation of the aldehyde's carbonyl site, the isotope effect is assumed to only occur on the C-1 carbon, so the molecular-average $\delta^{13}C$ for acetic acid was calculated accounting for the isotope effect only occurring on this site (Eqn. A3). Higher carbon chain carboxylic acids (C_2 and above) were calculated as the carbon-weighted average values of acetaldehyde (64.6 ± 1.5 ‰) and additional CH_x groups (-36 ± 10 ‰) to decrease error (Eqn. A4).

$$^{13}R_{\text{molec avg, acetic acid}} = (1\text{-}0.050/2)\ ^{13}R_{\text{molec avg, acetaldehyde}} \quad (A3)$$

$$^{13}F_{\text{C-x-carboxylic acid}} = \left(\frac{2}{x}\right)^{13}F_{\text{molec avg, acetic acid}} + \left(\frac{x-2}{x}\right)\ ^{13}F_{\text{C-2, acetaldehyde}} \quad (A4)$$

All α-amino acids (*i.e.* not only alanine) were assumed to undergo fractionation in Strecker synthesis as described above. Because our analytical Murchison alanine measurements include $\delta^{13}C$ for sites that have undergone the same fractionations associated with their synthesis (*e.g.*, the C-1 and C-2 carbons of all alpha amino acids formed by Strecker synthesis are predicted to be fractionated in the same way we predict for our model of alanine formation), we used alanine's site-specific isotopic composition as our building blocks for other amino acids. Glycine's $\delta^{13}C$ was predicted based on the 184.021 *m/z* fragment measurement (corrected for dilution with carbons from derivatizing agents) and alanine was assigned to have the $\delta^{13}C$ value directly measured in this study, 25.5 ‰ (*e.g.*, it is not predicted but serves as the basis for predicting other species, particularly acetaldehyde and HCN). All amino acids with longer alkyl chains than alanine were assumed to have additional alkyl carbons (*i.e.:* with a $\delta^{13}C$ equal to that of C-3 in alanine) comprising the balance of the molecular carbon inventory (Eqn. A5).

$$^{13}F_{\text{Cx-amino acid}} = \left(\frac{3}{x}\right)^{13}F_{\text{molec avg, alanine}} + \left(\frac{x-3}{x}\right)\ ^{13}F_{\text{C3, alanine}} \quad (A5)$$

In addition to Strecker synthesis, we also considered the possibility that C-1 in amino acids could equilibrate with the dissolved inorganic carbon (DIC) pool on meteorites (*e.g.*, the carbonate pool). The DIC pool is 3000 times more abundant than all amino acids on Murchison combined (Sephton, 2002). Consequently, in the case of equilibration between the two reservoirs, the $\delta^{13}C$

value of DIC would control that of C-1 in amino acids. We assumed a DIC reservoir with a $\delta^{13}C$ of 80 ‰, equal to the highest measured literature value for CM chondrites (Sephton, 2002) (and thus the maximum effect on amino acids with which it equilibrates). Using ε values for CO_3^{2-}-CO_2 and CO_2-amino acid carboxyl group equilibration from (Rustad et al., 2008) and (Rustad, 2009) respectively, we predicted the $\delta^{13}C$ of different amino acids on Murchison that had equilibrated with its carbonate pool (Dataset S2). Of amino acids with molecular-average $\delta^{13}C$ values measured on Murchison, only glycine and alanine also have ε values for CO_2 and amino acid carboxyl group in (Rustad, 2009). These values are 4.4 ‰ and 4.9 ‰, so we adopted an average value of 4.65 ‰ for $\varepsilon_{CO2\text{-amino acid C-1 site}}$ in our calculations for all amino acids.

Bibliography

Abelson P. H. and Hoering T. C. (1961) Carbon isotope fractionation in formation of amino acids by photosynthetic organisms. *Proc. Natl. Acad. Sci. USA* **47**, 623–632.

Billault I., Courant F., Pasquereau L., Derrien S., Robins R. J. and Naulet N. (2007) Correlation between the synthetic origin of methamphetamine samples and their ^{15}N and ^{13}C stable isotope ratios. *Anal. Chim. Acta* **593**, 20–29.

Biver N., Bockelée-Morvan D., Hofstadter M., Lellouch E., Choukroun M., Gulkis S., Crovisier J., Schloerb F. P., Rezac L., von Allmen P., Lee S., Leyrat C., Ip W. H., Hartogh P., Encrenaz P., Beaudin G. and the MIRO team (2019) Long-term monitoring of the outgassing and composition of comet 67P/Churyumov-Gerasimenko with the Rosetta/MIRO instrument. *A&A* **630**, A19.

Canellas P. F. and Cleland W. W. (1991) Carbon-13 and deuterium isotope effects on the reaction catalyzed by glyceraldehyde-3-phosphate dehydrogenase. *Biochemistry* **30**, 8871–8876.

Cleland W. W. (2005) The use of isotope effects to determine enzyme mechanisms. *Arch. Biochem. Biophys.* **433**, 2–12.

Eiler J., Cesar J., Chimiak L., Dallas B., Grice K., Griep-Raming J., Juchelka D., Kitchen N., Lloyd M., Makarov A., Robins R. and Schwieters J. (2017) Analysis of molecular isotopic structures at high precision and accuracy by Orbitrap mass spectrometry. *Int. J. Mass Spectrom.* **422**, 126–142.

Elsila J. E., Charnley S. B., Burton A. S., Glavin D. P. and Dworkin J. P. (2012) Compound-specific carbon, nitrogen, and hydrogen isotopic ratios for amino acids in CM and CR chondrites and their use in evaluating potential formation pathways. *Meteorit. Planet. Sci.* **47**, 1517–1536.

Gilbert A., Silvestre V., Segebarth N., Tcherkez G., Guillou C., Robins R. J., Akoka S. and Remaud G. S. (2011) The intramolecular ^{13}C-distribution in ethanol reveals the influence of the CO_2 -fixation pathway and environmental conditions on the site-specific ^{13}C variation in glucose. *Plant Cell Environ.* **34**, 1104–1112.

Guo W. and Eiler J. M. (2007) Temperatures of aqueous alteration and evidence for methane generation on the parent bodies of the CM chondrites. *Geochim. Cosmochim. Acta* **71**, 5565–5575.

Huang Y., Alexandre M. R. and Wang Y. (2007) Structure and isotopic ratios of aliphatic side chains in the insoluble organic matter of the Murchison carbonaceous chondrite. *Earth Planet. Sci. Lett.* **259**, 517–525.

Lynn K. R. and Yankwich P. E. (1961) Cyanide Carbon Isotope Fractionation in the Reaction of Cyanide Ion and Methyl Iodide. Carbon Isotope Effect in the Hydrolysis of Methyl Iodide. *J. Am. Chem. Soc.* **83**, 53–57.

Neubauer C., Sweredoski M. J., Moradian A., Newman D. K., Robins R. J. and Eiler J. M. (2018) Scanning the isotopic structure of molecules by tandem mass spectrometry. *Int. J. Mass Spectrom.* **434**, 276–286.

Pizzarello S. (2014) The Nitrogen Isotopic Composition of Meteoritic HCN. *Astrophys. J.* **796**, L25.

Robins L. I., Fogle E. J. and Marlier J. F. (2015) Mechanistic investigations of the hydrolysis of amides, oxoesters and thioesters via kinetic isotope effects and positional isotope exchange. *Biochimica et Biophysica Acta (BBA)-Prot. Proteom.* **1854**, 1756–1767.

Rustad J. R. (2009) Ab initio calculation of the carbon isotope signatures of amino acids. *Org. Geochem.* **40**, 720–723.

Rustad J. R., Nelmes S. L., Jackson V. E. and Dixon D. A. (2008) Quantum-chemical calculations of carbon-isotope fractionation in CO2(g), aqueous carbonate species, and carbonate minerals. *J. Phys. Chem. A* **112**, 542–555.

Sephton M. A. (2002) Organic compounds in carbonaceous meteorites. *Nat. Prod. Rep.* **19**, 292–311.

Van Slyke D. D., Dillon R. T., MacFadyen D. A. and Hamilton P. (1941) Gasometric Determination of Carboxyl Groups in Free Amino Acids. *J. Bio. Chem.* **141**, 627–669.

Wiberg K. B. (1954) The deuterium isotope effect of some ionic reactions of benzaldehyde. *J. Am. Chem. Soc.* **76**, 5371–5375.

Yuen G., Blair N., Des Marais D. J. and Chang S. (1984) Carbon isotope composition of low molecular weight hydrocarbons and monocarboxylic acids from Murchison meteorite. *Nature* **307**, 252–254.

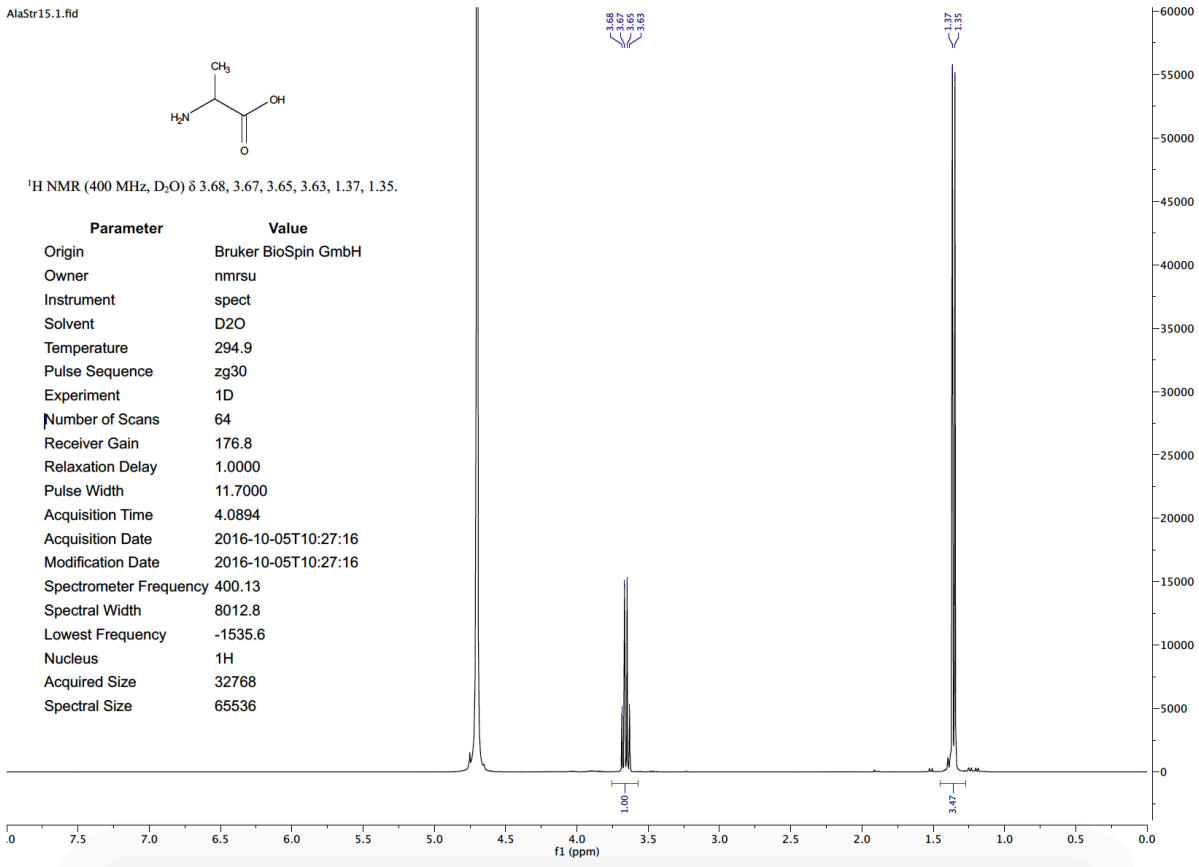

Figure S1: NMR of Strecker Alanine standard.

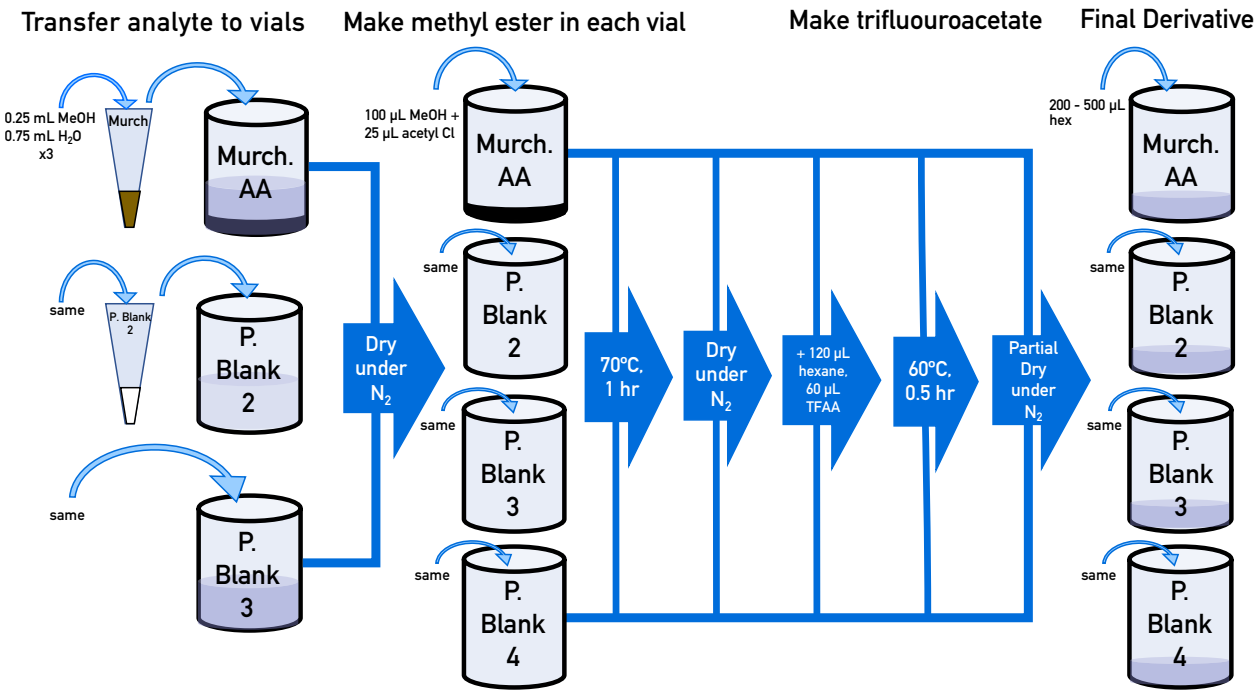

Figure S2: Steps in derivatization of samples, standards, and blanks.

(a)

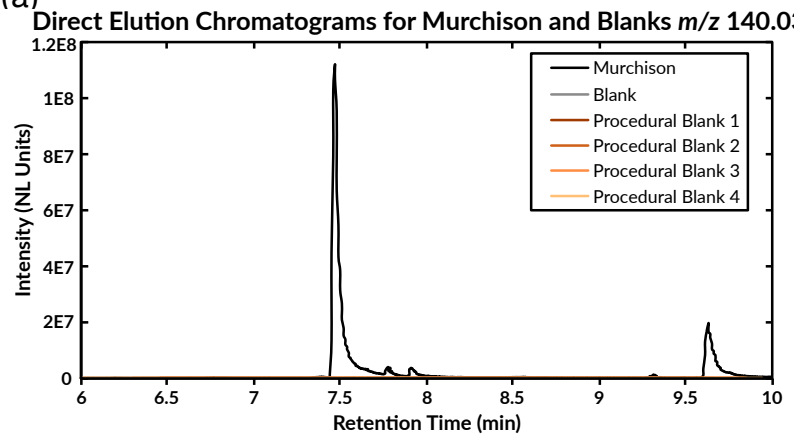
Direct Elution Chromatograms for Murchison and Blanks m/z 140.032
Intensity (NL Units)
Retention Time (min)
Murchison
Blank
Procedural Blank 1
Procedural Blank 2
Procedural Blank 3
Procedural Blank 4

(b)

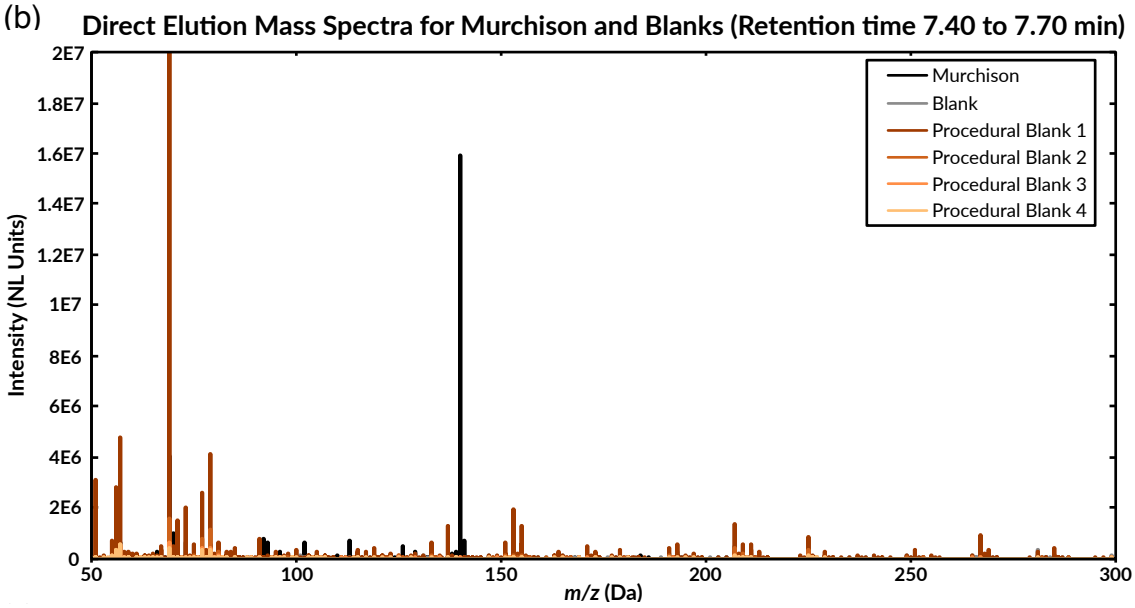
Direct Elution Mass Spectra for Murchison and Blanks (Retention time 7.40 to 7.70 min)
Intensity (NL Units)
m/z (Da)
Murchison
Blank
Procedural Blank 1
Procedural Blank 2
Procedural Blank 3
Procedural Blank 4

(c)

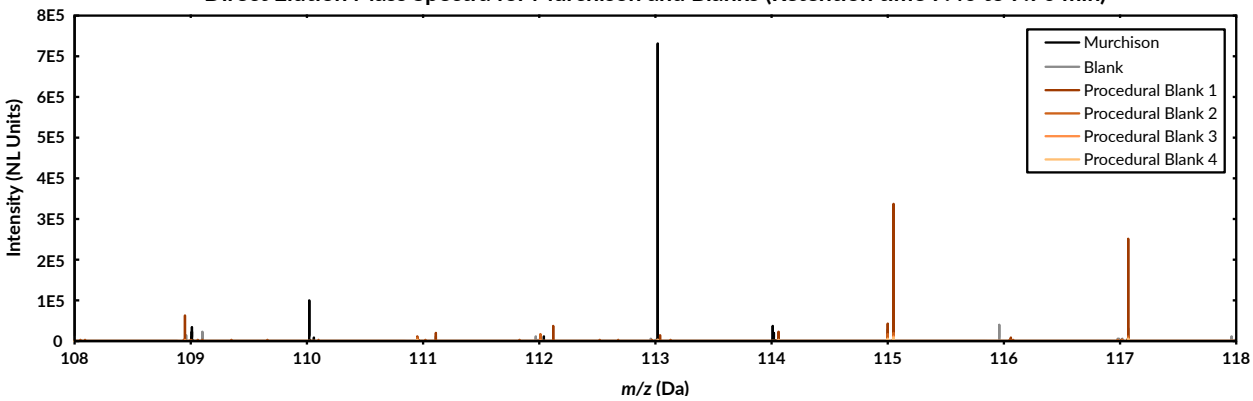
Direct Elution Mass Spectra for Murchison and Blanks (Retention time 7.40 to 7.70 min)
Intensity (NL Units)
m/z (Da)
Murchison
Blank
Procedural Blank 1
Procedural Blank 2
Procedural Blank 3
Procedural Blank 4

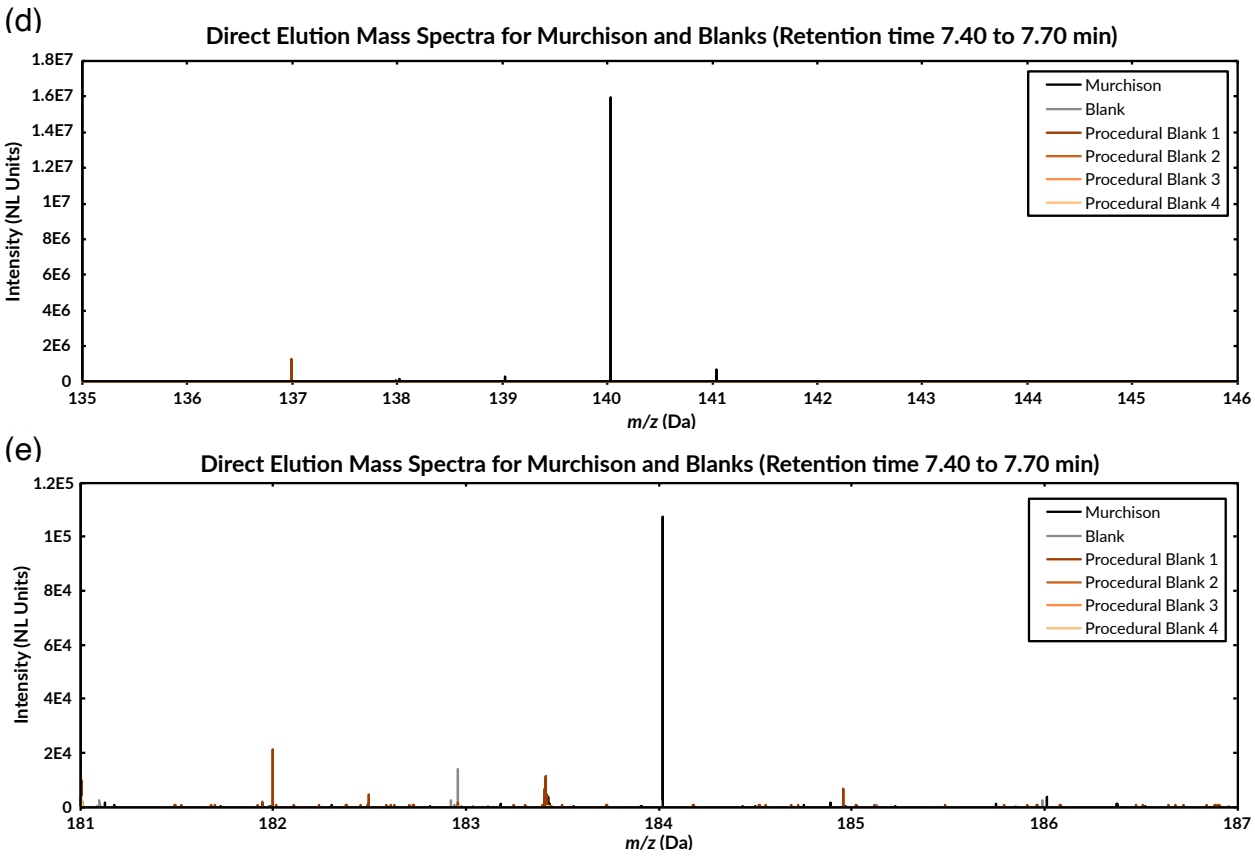

Figure S3: Gas chromatograms and mass spectra for the analytical Murchison sample. (a) Mass spectra from *m/z* 50-300 for Murchison sample and blanks. (b) Chromatogram for the *m/z* 140.032 trace (the main fragment for alanine) for Murchison sample and blanks from 5 to 10 minutes. (c) Mass spectra from *m/z* 108-118 (113 fragment measurement window) for Murchison sample and blanks. (d) Mass spectra from *m/z* 135-146 (140 fragment measurement window) for Murchison sample and blanks. (e) Mass spectra from *m/z* 181-187 (184 fragment measurement window) for Murchison sample and blanks. Retention time for the mass spectra capture the alanine derivative's elution time.

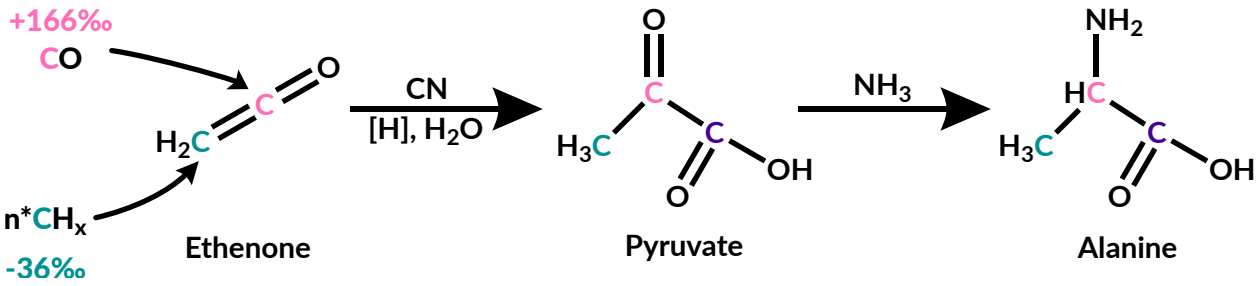

Figure S4: Ketene reaction mechanism to create alanine with a similar carbon isotope structure to the one measured in this paper. Pyruvate is created in the ISM and can react with NH_3 either in the ISM or on a parent body in the solar nebula.

Sample (p*mol ala/μL*)	Procedural Blank #	First Step	% of signal relative to Murchison			*Max pmol ala/μL*
			Σ12C Counts	Σ13C Counts	Σ12C Intensity	
Methods Development Murchison, January 2018 (29)	Hexane	Pure Hexane	0.1%	0.0%	0.0%	0.11
	1	Transfer of Meteorite to GC vial Run Prior to Derivatization	0.5%	0.1%	0.2%	0.45
	2	Extraction of meteorite at NASA	0.8%	0.2%	0.2%	2.4
	3	Transfer of Meteorite to GC vial	0.3%	0.0%	0.1%	1.0
Methods Development Murchison, March 2018 (29)	Hexane	Pure Hexane	0.0%	0.1%	0.0%	3.1×10^{-3}
	1	Transfer of Meteorite to GC vial Run Prior to Derivatization	0.2%	0.1%	0.1%	5.4×10^{-2}
	2	Extraction of meteorite at NASA	1.0%	0.0%	0.3%	0.29
	3	Transfer of Meteorite to GC vial	5.6%	3.4%	3.7%	1.6
Analytical Murchison, Summer 2018 (15)	Hexane	Pure Hexane	0.0%	0.0%	0.0%	1.3×10^{-3}
	1	Transfer of Meteorite to GC vial Run Prior to Derivatization	0.0%	0.0%	0.1%	1.8×10^{-3}
	2	Extraction of meteorite at NASA	1.0%	0.0%	0.2%	0.16
	3	Transfer of Meteorite to GC vial	0.7%	0.0%	0.1%	9.8×10^{-2}
	4	Chemical Derivatization	0.5%	0.0%	0.0%	6.9×10^{-2}

Table S1. Blank IDs and possible contamination to Murchison.

Analysis Set	Date	Scan Range	% of signal relative to alanine		Maximum ‰ change in ^{13}R
			$\Sigma^{12}C$ Counts	$\Sigma^{13}C$ Counts	
Methods Development Murchison, January 2018	1/3	135-146 *RE*	0.08%	0.05%	-0.061
	1/3	135-146 *RE*	0.31%	0.29%	-0.037
	1/3	135-146 *RE*	0.16%	0.14%	-0.027
	1/4	50-300 *DE*	0.00%	0.00%	0.000
	1/6	50-300 *DE*	0.04%	0.00%	-0.091
	1/7	50-300 *DE*	0.09%	0.00%	-0.086
	1/7	50-300 *DE*	0.31%	0.10%	-0.210
	1/7	181-187 *RE*	0.00%	0.05%	0.048
Methods Development Murchison, March 2018	3/26	50-500 *DE*	0.0%	0.0%	-0.002
	3/26	50-500 *DE*	0.0%	0.0%	-0.007
	3/27	135-146 *RE*	0.0%	0.0%	0.000
	3/29	181-187 *RE*	0.0%	0.2%	0.199
	3/30	181-187 *RE*	0.0%	0.3%	0.282
	3/31	181-187 *RE*	0.0%	2.8%	2.756
Analytical Murchison, Summer 2018	6/27	135-146 *RE*	0.12%	0.12%	-0.002
	6/27	135-146 *RE*	0.12%	0.11%	-0.010
	6/27	135-146 *RE*	0.16%	0.16%	-0.002
	7/12	181-187 *RE*	0.52%	0.49%	-0.033
	7/12	181-187 *RE*	0.00%	0.07%	0.045
	7/12	181-187 *RE*	0.04%	0.01%	-0.033
	7/13	181-187 *RE*	0.05%	0.04%	-0.013
	7/16	108-118 *RE*	5.52%	6.20%	0.644

Table S2. Background from blanks during measurement. RE denotes samples analyzed using Reservoir Elution mode while DE denotes samples analyzed using Direct Elution mode.

Analysis Set	Sample	Analysis Number used	
		140	**184**
Winter 2018	Alfa Aesar	28, 29	47-49, 51-53, 61-62
	Strecker	30	64-67
	Methods Development Murchison	24-25	45-46, 55-59
Spring 2018	Alfa Aesar	75, 83	94, 97-99, 104
	Strecker	74, 80	x
	Methods Development Murchison	78, 84-86	101-103, 105-106
Summer 2018	Alfa Aesar	128, 131, 134-137	162, 166-167
	Strecker	139-140	159, 161
	Analytical Murchison	142, 144, 147	164-165

Table S3. Analysis numbers of measurements used to calculate ^{13}R values from samples and standards. Analysis numbers correspond to values found in Dataset S1 and were used to calculate ratios found in Table S2.

Date	Analysis #	Mass Range	Sample	Major Beam	Σ^{12}C Counts[a]	Σ^{13}C Counts[a]	^{13}R	*st err*
12/25/17	1	50-500	Hexane Blank	140	2.8E+02	1.0E+01	x	*x*
	2	50-500	Procedural Blank 1a	140	4.1E+02	3.3E+02	8.67695	*x*
	3	50-500	Procedural Blank 1a	140	1.0E+03	3.5E+02	0.03914	*x*
	4	50-500	Procedural Blank 1a	140	1.2E+03	4.1E+02	0.43825	*x*
	5	50-500	Procedural Blank 1a	140	1.7E+03	3.6E+01	0.03485	*0.00785*
	6	50-500	Hexane Blank	140	1.1E+03	4.5E+02	0.06308	*x*
12/28/17	7	50-500	Hexane Blank	140	8.4E+01	1.1E+01	x	*x*
	8	50-500	Procedural Blank 1b	140	3.5E+03	7.4E+01	0.00001	*0.00698*
	9	50-500	Hexane Blank	140	1.5E+01	0.0E+00	x	*x*
	10	50-500	Hexane Blank	140	9.1E+01	5.0E+00	x	*x*
	11	50-500	Hexane Blank	140	1.1E+03	1.1E+01	0.05422	*0.00560*
	12	50-500	Hexane Blank	140	1.9E+03	3.5E+01	0.04713	*0.00536*
	13	50-500	Procedural Blank 1b	140	7.9E+02	4.9E+00	x	*x*
	14	50-500	Hexane Blank	140	1.9E+03	1.8E+01	0.09737	*0.01377*
12/29/17	15	50-500	Hexane Blank	140	2.0E+02	0.0E+00	x	*x*
	16	50-500	Procedural Blank 3	140	5.8E+02	0.0E+00	x	*x*
	17	50-500	Procedural Blank 2	140	1.4E+03	1.6E+01	0.04341	*0.00271*
	18	50-500	Murchison Direct	140	1.7E+05	6.6E+03	0.04323	*0.00136*
1/3/18	19	135-146	Hexane Blank	140	1.3E+03	0.0E+00	x	*x*
	20	135-146	Hexane Blank	140	3.3E+04	7.2E+02	0.03735	*0.00166*
	21	135-146	No Injection	140	1.2E+04	1.2E+02	0.06482	*0.00623*
	22	135-146	Alfa Aesar[x]	140	6.8E+06	2.9E+05	0.04298	*0.00008*
	23	135-146	Hexane Blank	140	2.2E+04	5.2E+02	0.04069	*0.00286*

Winter 2018		24	135-146	Murchison	140	1.7E+07	7.7E+05	0.04385	*0.00006*
		25	135-146	Murchison	140	2.1E+07	9.2E+05	0.04374	*0.00006*
		26	135-146	Hexane Blank	140	8.2E+04	3.3E+03	0.04280	*0.00136*
		27	135-146	DCM Blank	140	4.0E+04	1.4E+03	0.04039	*0.00192*
		28	135-146	Alfa Aesar	140	1.8E+07	7.6E+05	0.04309	*0.00006*
		29	135-146	Alfa Aesar	140	2.0E+07	8.5E+05	0.04318	*0.00006*
		30	135-146	Strecker	140	4.2E+07	1.8E+06	0.04297	*0.00004*
	1/4/18	31	50-300	Hexane Blank	140	5.3E+00	0.0E+00	x	*x*
		32	50-300	Hexane Blank	140	3.2E+01	0.0E+00	x	*x*
		33	50-300	DCM Blank	140	0.0E+00	0.0E+00	x	*x*
		34	50-300	No Injection	140	9.6E+00	0.0E+00	x	*x*
		35	50-300	No Injection	140	4.7E+00	0.0E+00	x	*x*
		36	50-300	No Injection	140	5.4E+00	0.0E+00	x	*x*
		37	50-300	No Injection	140	0.0E+00	0.0E+00	x	*x*
		38	181-187	Murchison	184	2.4E+05	1.2E+04	x	*x*
		39	181-187	Alfa Aesar 2	184	6.7E+05	3.7E+04	0.05491	*0.00040*
		40	181-187	Procedural Blank 3	184	1.1E+01	9.9E+00	x	*x*
	1/5/18	41	181-187	Murchison Direct	184	*1.6E+05*	*1.3E+04*	x	*x*
		42	50-500	Murchison Direct	140	*7.1E+05*	*1.9E+04*	x	*x*
		43	181-187	Murchison Direct	184	2.0E+05	1.3E+04	x	*x*
	1/6/18	44	50-300	Murchison	140	2.4E+06	9.7E+04	0.04160	*0.00035*
		45	181-187	Murchison	184	5.3E+05	3.2E+04	0.05510	*0.00055*
		46	181-187	Murchison	184	4.6E+05	2.8E+04	0.05484	*0.00051*
		47	181-187	Alfa Aesar	184	5.3E+05	2.8E+04	0.05409	*0.00047*
		48	181-187	Alfa Aesar	184	6.6E+05	3.5E+04	0.05354	*0.00044*
		49	181-187	Alfa Aesar	184	5.8E+05	3.1E+04	0.05434	*0.00051*
		50	50-300	Hexane Blank	140	4.5E+02	0.0E+00	x	*x*
		51	181-187	Alfa Aesar	184	4.7E+05	2.4E+04	0.05415	*0.00074*
		52	181-187	Alfa Aesar	184	5.5E+05	2.9E+04	0.05351	*0.00057*
		53	181-187	Alfa Aesar	184	5.5E+05	2.9E+04	0.05360	*0.00052*

		54	50-300	Hexane Blank	140	4.4E+02	0.0E+00	x	*x*
		55	181-187	Murchison	184	5.2E+05	3.1E+04	0.05442	*0.00054*
		56	181-187	Murchison	184	4.6E+05	2.7E+04	0.05421	*0.00056*
		57	181-187	Murchison	184	4.7E+05	2.8E+04	0.05441	*0.00055*
		58	181-187	Murchison	184	5.5E+05	3.3E+04	0.05451	*0.00046*
	1/7/18	59	181-187	Murchison	184	5.3E+05	3.2E+04	0.05457	*0.00049*
		60	50-300	Hexane Blank	140	2.0E+03	3.5E+01	0.03361	*0.00462*
		61	181-187	Alfa Aesar	184	6.6E+05	3.5E+04	0.05356	*0.00042*
		62	181-187	Alfa Aesar	184	6.0E+05	3.2E+04	0.05460	*0.00045*
		63	181-187	Hexane Blank	184	4.0E+01	4.5E+01	x	*x*
		64	181-187	Strecker	184	2.3E+06	1.2E+05	0.05390	*0.00021*
		65	181-187	Strecker	184	1.8E+06	9.8E+04	0.05389	*0.00022*
		66	181-187	Strecker	184	1.9E+06	1.0E+05	0.05387	*0.00022*
		67	181-187	Strecker	184	6.3E+05	3.2E+04	0.05294	*0.00043*
		68	50-500	Procedural Blank 1a	140	2.5E+03	8.5E+00	0.08129	*N/A*
		69	50-500	Procedural Blank 3	140	3.0E+03	0.0E+00	N/A	*N/A*
	3/23/18	70	50-500	Procedural Blank 2	140	1.7E+04	4.1E+02	0.04554	*0.03297*
		71	50-500	Murchison Direct	140	3.0E+05	1.2E+04	x	*x*
		72	50-500	Procedural Blank 2	140	5.6E+02	0.0E+00	N/A	*N/A*
		73	135-146	Alfa Aesar[x]	140	2.9E+07	1.3E+06	0.04312	*0.00007*
		74	135-146	Strecker[x]	140	7.8E+07	3.4E+06	0.04284	*0.00003*
	3/26/18	75	135-146	Alfa Aesar	140	3.6E+07	1.6E+06	0.04324	*0.00004*
		76	50-500	Hexane Blank	140	1.2E+03	0.0E+00	N/A	*N/A*
		77	135-146	Murchison	140	9.8E+06	4.2E+05	0.04339	*0.00011*
		78	135-146	Murchison	140	2.2E+07	9.8E+05	0.04381	*0.00006*
		79	135-146	Alfa Aesar[x]	140	2.8E+07	1.2E+06	0.04329	*0.00005*
		80	135-146	Strecker[x]	140	6.6E+07	2.8E+06	0.04296	*0.00004*
		81	135-146	Alfa Aesar[x]	140	3.2E+07	1.4E+06	0.04318	*0.00005*
	3/27/18	82	135-146	Blank No Injection	140	8.4E+03	3.9E+02	0.06179	*0.00555*
		83	135-146	Alfa Aesar	140	2.6E+07	1.1E+06	0.04320	*0.00006*
		84	135-146	Murchison	140	2.3E+07	1.0E+06	0.04381	*0.00007*
		85	135-146	Murchison	140	2.3E+07	1.0E+06	0.04392	*0.00007*

Spring 2018		86	135-146	Murchison	140	2.3E+07	1.0E+06	0.04379	*0.00006*
		87	135-146	Alfa Aesar[x]	140	2.5E+07	1.1E+06	0.04335	*0.00010*
		88	181-187	Alfa Aesar	184	1.9E+05	9.9E+03	x	*x*
		89	181-187	Alfa Aesar	184	2.3E+05	1.2E+04	x	*x*
	3/29/18	90	181-187	Blank No Injection	184	0.0E+00	4.3E+01	x	*x*
		91	181-187	Murchison	184			x	*x*
		92	181-187	Murchison	184	3.6E+05	2.2E+04	x	*x*
		93	181-187	Alfa Aesar	184	5.7E+05	3.1E+04	x	*x*
		94	181-187	Alfa Aesar	184	1.1E+05	5.9E+03	0.05440	*0.00059*
		95	181-187	Alfa Aesar	184	6.8E+05	3.7E+04	0.05536	*0.00047*
		96	181-187	Alfa Aesar	184	6.2E+05	3.8E+04	x	*x*
		97	181-187	Alfa Aesar	184	5.9E+05	3.7E+04	0.05272	*0.0007*
	3/30/18	99	181-187	Alfa Aesar	184	4.1E+05	2.1E+04	0.05452	*0.00068*
		99	181-187	Alfa Aesar	184	4.1E+05	2.1E+04	0.05487	*0.00040*
		100	181-187	Blank No Injection	184	9.1E+00	6.1E+01	x	*x*
		101	181-187	Murchison	184	3.5E+05	2.1E+04	0.05437	*0.00056*
		102	181-187	Murchison	184	3.5E+05	2.1E+04	0.05513	*0.00066*
		103	181-187	Murchison	184	3.5E+05	2.1E+04	0.05537	*0.00069*
		104	181-187	Alfa Aesar	184	4.2E+05	2.2E+04	0.05377	*0.00064*
		105	181-187	Murchison	184	3.4E+05	2.2E+04	0.05538	*0.00069*
		106	181-187	Murchison	184	3.0E+05	1.9E+04	0.05511	*0.00084*
		107	181-187	Alfa Aesar	184	6.8E+05	3.6E+04	0.05434	*0.00044*
	3/31/18	108	181-187	Blank No Injection	184	1.9E+02	1.1E+03	2.57453	*0.38971*
		109	181-187	Murchison	184	6.7E+05	4.1E+04	0.05575	*0.00040*
		110	181-187	Murchison	184	6.2E+05	3.8E+04	0.05575	*0.00053*
		111	181-187	Murchison	184	5.9E+05	3.7E+04	0.05600	*0.00049*
		112	181-187	Alfa Aesar	184	2.1E+05	1.1E+04	0.05453	*0.00035*
		113	181-187	Alfa Aesar	184	2.1E+05	1.1E+04	0.05448	*0.00036*
Summer 2018									
		114	50-300	Hexane Blank	140	1.6E+04	5.9E+01	0.08947	*0.05274*
		115	50-300	Hexane Blank	140	4.6E+01	6.7E+00	x	*x*
	6/13/18	116	50-300	Procedural Blank 1b	140	0.0E+00	0.0E+00	x	*x*
		117	50-300	Procedural Blank 1b	140	2.4E+02	1.8E+03	2.01979	*0.08559*
		118	50-300	Procedural Blank 1b	140	1.5E+02	0.0E+00	x	*x*

6/14/18	119	50-300	Hexane Blank	140	3.8E+01	0.0E+00	x	*x*
	120	50-300	Hexane Blank	140	1.4E+01	0.0E+00	x	*x*
	121	50-300	Procedural Blank 2	140	3.6E+03	0.0E+00	x	*x*
	122	50-300	Murchison, Direct	140	3.3E+05	1.3E+04	x	*x*
6/15/18	123	50-300	Hexane Blank	140	3.6E+03	0.0E+00	x	*x*
	124	50-300	Procedural Blank 4	140	1.6E+03	0.0E+00	x	*x*
	125	50-300	Procedural Blank 3	140	2.2E+03	0.0E+00	x	*x*
	126	50-300	Procedural Blank 2	140	6.2E+03	8.9E+01	0.05664	*x*
6/25/18	127	135-146	Alfa Aesar[x]	140	4.1E+07	1.7E+06	0.04211	*0.00006*
	128	135-146	Alfa Aesar	140	3.4E+07	1.4E+06	0.04222	*0.00005*
	129	135-146	Alfa Aesar[x]	140	7.4E+07	3.1E+06	0.04211	*0.00003*
	130	135-146	Alfa Aesar[x]	140	8.3E+07	3.5E+06	0.04235	*0.00003*
	131	135-146	Alfa Aesar	140	4.3E+07	1.8E+06	0.04219	*0.00003*
	132	135-146	Alfa Aesar[x]	140	7.0E+07	3.0E+06	0.04223	*0.00004*
	133	135-146	Alfa Aesar[x]	140	7.4E+07	3.1E+06	0.04221	*0.00004*
6/26/18	134	135-146	Alfa Aesar	140	2.0E+07	8.5E+05	0.04242	*0.00007*
	135	135-146	Alfa Aesar	140	2.3E+07	9.5E+05	0.04205	*0.00007*
	136	135-146	Alfa Aesar	140	4.6E+07	2.0E+06	0.04270	*0.00004*
6/27/18	137	135-146	Alfa Aesar	140	4.7E+07	2.0E+06	0.04243	*0.00004*
	138	135-146	Alfa Aesar[x]	140	8.3E+07	3.5E+06	0.04253	*0.00003*
	139	135-146	Strecker	140	2.9E+07	1.2E+06	0.04205	*0.00006*
	140	135-146	Strecker	140	4.5E+07	1.9E+06	0.04202	*0.00004*
	141	135-146	Hexane Blank	140	3.3E+04	1.4E+03	0.04316	*x*
	142	135-146	Murchison	140	4.3E+07	1.9E+06	0.04372	*0.00005*
	143	135-146	Hexane Blank	140	3.6E+04	1.4E+03	0.03967	*x*
	144	135-146	Murchison	140	3.6E+07	1.6E+06	0.04372	*0.00005*
	145	135-146	Alfa Aesar[x]	140	8.3E+07	3.5E+06	0.04249	*0.00003*

	146	135-146	Hexane Blank	140	4.5E+04	2.0E+03	0.04303	*x*
	147	135-146	Murchison	140	4.0E+07	1.7E+06	0.04368	*0.00004*
7/9/18	148	108-118	Alfa Aesar[x]	113	1.2E+07	3.6E+05	0.03147	*0.00011*
	149	181-187	Alfa Aesar	184	5.2E+06	2.9E+05	0.05573	*0.00016*
	150	181-187	Alfa Aesar	184	6.6E+06	3.7E+05	0.05627	*0.00015*
7/10/18	151	108-118	Alfa Aesar[x]	113	1.4E+07	4.6E+05	0.03159	*0.00009*
	152	108-118	Alfa Aesar[x]	113	7.3E+06	2.3E+05	0.03124	*0.00012*
	153	181-187	Alfa Aesar	184	2.8E+06	1.4E+05	0.05400	*0.00040*
7/11/18	154	181-187	Alfa Aesar	184	3.3E+06	1.7E+05	0.05489	*0.00028*
	155	181-187	Strecker	184	2.4E+06	1.2E+05	0.05462	*0.00032*
	156	181-187	Hexane Blank	184	2.2E+04	1.1E+03	0.05291	
	157	181-187	Alfa Aesar	184	4.0E+06	2.2E+05	0.05544	*0.00017*
	158	181-187	Alfa Aesar	184	4.3E+06	2.4E+05	0.05572	*0.00016*
	159	181-187	Strecker	184	3.9E+06	2.1E+05	0.05493	*0.00018*
	160	181-187	Hexane Blank	184	2.9E+01	9.7E+01	N/A	
7/12/18	161	181-187	Strecker	184	2.1E+06	1.1E+05	0.05455	*0.00024*
	162	181-187	Alfa Aesar	184	5.5E+06	3.1E+05	0.05598	*0.00014*
	163	181-187	Hexane Blank	184	9.5E+02	1.0E+01	0.38462	
	164	181-187	Murchison	184	2.5E+06	1.4E+05	0.05762	*0.00025*
	165	181-187	Murchison	184	2.2E+06	1.3E+05	0.05664	*0.00023*
	166	181-187	Alfa Aesar	184	1.8E+06	9.6E+04	0.05471	*0.00028*
	167	181-187	Alfa Aesar	184	3.4E+06	1.8E+05	0.05461	*0.00017*
	168	181-187	Strecker	184	1.5E+06	8.1E+04	0.05376	*0.00034*
	169	181-187	Alfa Aesar	184	9.7E+05	5.1E+04	0.05433	*0.00052*
	170	181-187	Alfa Aesar	184	1.4E+06	7.3E+04	0.05406	*0.00031*
7/13/18	171	181-187	Hexane Blank	184	1.1E+03	4.7E+01	0.43118	*x*
	172	181-187	Murchison	184	1.7E+06	9.4E+04	0.05707	*0.00032*
	173	181-187	Murchison	184	2.3E+06	1.3E+05	0.05708	*0.00025*
	174	181-187	Murchison	184	2.1E+06	1.2E+05	0.05789	*0.00028*
	175	108-118	Alfa Aesar	113	3.5E+06	1.1E+05	0.03131	*0.00015*
	176	108-118	Strecker	113	4.5E+06	1.4E+05	0.03119	*0.00017*
	177	108-118	Strecker	113	4.6E+06	1.4E+05	0.03126	*0.00016*

	7/16/18	178	108-118	Hexane Blank	113	6.2E+04	1.8E+03	0.03139	*x*
		179	108-118	Murchison[s]	113	1.3E+06	4.2E+04	0.03167	*0.00020*
		180	108-118	Murchison[s]	113	1.4E+06	3.9E+04	0.03137	*0.00020*
		181	108-118	Alfa Aesar	113	4.0E+06	2.3E+05	0.03103	*0.00013*
		182	108-118	Alfa Aesar	113	5.3E+06	1.6E+05	0.03098	*0.00013*

[a]Note: Σ^{12}C Counts and Σ^{13}C Counts are summed over all scans from 6.5 to 8.5 minutes including those with only a monoisotopic or only a singly ^{13}C subsistuted peak. They will not necessarily divide to equal ^{13}R, which is calcualted using only scans with both the monosiotopic and singly ^{13}C subsituted peaks.

[x] sample for which TICxIT oscillated/was unstable

[s] sample for which alanine was captured in addition to a subsequent peak

	Molecule	Carbon #	Measurements, This Paper	Predictions	Predictions (Alternate)	Literature
Alanine Sites	C-1	1	-25.7 ± 9.3			
	C-2	1	138.5 ± 9.7			
	C-3	1	-36.3 ± 10.0			
Precursor Sites	CN	1		-6.7 ± 9.5		5 ± 10[a]
	CO	1		165.5 ± 9.9		
	CH_x	1		-36.3 ± 10.4		
Aldehydes	formaldehyde	1		165.5 ± 9.9		
	acetaldehyde	2		64.6 ± 1.5		25.7 ± 0.9 (*E*)[b], 27.0 ± 0.9 (*Z*)[b], 64 ± 1[c]
	propoanal	3		31.0 ± 3.6		41.8 ± 1.3 (*Z*)[b], 47 ± 6[c]
	butanal	4		14.1 ± 5.2		20.3 ± 1.3 (*E*)[b], 3 ± 2[c]
	pentanal	5		4.1 ± 6.3		5 ± 5[c]
	hexanal	6		-2.7 ± 6.9		-1 ± 7[c]
	isobutanal	4*		14.1 ± 5.2		40 ± 2[c]
	isopentanal	5*		4.1 ± 6.3		36 ± 3[c]
Amines	methylamine	1		165.5 ± 9.9		129 ± 7[d]
	ethylamine	2		64.6 ± 1.5		80 ± 2[d]
	N--propylamine	3		31.0 ± 3.6		40 ± 1[d]
	N--butylamine	4		14.1 ± 5.2		43 ± 2[d]
Carboxylic Acids	acetic	2		64.6 ± 1.5	48.7 ± 1.5	22.7 ± 0.2[e], -7.7 ± 0.2[f], -52.1 ± 1[g]
	propanoic	3		31.0 ± 3.6	20.3 ± 3.6	17.4 ± 0.2[e], 7.3 ± 1.6[f], -1 ± 1[g]
	butyric	4		14.1 ± 5.2	6.2 ± 5.2	11 ± 0.2[e], 0 ± 0.4[f], -4 ± 3[g]
	valeric	5		4.1 ± 6.3	-2.3 ± 6.3	4.5 ± 0.2[e], -10.4 ± 0.3[f], -9 ± 2[g]
	hexanoic	6		-2.7 ± 6.9	-8.0 ± 6.9	-18.3 ± 0.1[f], -17 ± 2[g]
α-H-Amino Acids	glycine	2		56.4 ± 8.9	107.8 ± 8.9	22[h], 40.5 ± 2.3[i], 13 ± 3[j]
	alanine	3	25.5 ± 3	25.5 ± 3	59.8 ± 3	28.5[h], 45.1± 1.9[i], 39 ± 3[j]
	aminobutyric	4		10.0 ± 3.4	35.7 ± 3.4	28.45 ± 0.6[i]
	norvaline	5		0.8 ± 4.5	21.3 ± 4.5	15.2[i]
α-CH3-Amino Acids	α-amino isobutyric acid	4		10.0 ± 3.4	35.7 ± 3.4	5[h], 43.1 ± 1.6[i], 28± 4[j]
	Isovaline	5		0.8 ± 4.5	21.3 ± 4.5	17[h], 22.1 ± 1.3[i], 39 ± 2[j]
	2-methylnorval	6		-5.4 ± 5.4	17.9 ± 5.4	6.8 ± 1.4[i]
	2-amino-2,3-dimethylbutyric acid	6*		-5.4 ± 5.4	17.4 ± 5.4	22.9 ± 0.7[i]

Literature values are from (a) Pizzarello et al. (2014)(*25*), (b) Simkus et al. (2019)(*24*), (c) Aponte et al. (2019)(*23*), (d) Aponte et al. (2016)(*27*), (e) Yuen et al. (1984)(*13*), (f) Huang et al. (2005)(*33*), (g) Aponte et al. (2019)(*34*), (h) Engel et al. (1990)(*1*), (i) Pizzarello et al. (2004)(*35*), (j) Elsila et al. (2012)(*11*).